Monthly Notices of the ROYAL ASTRONOMICAL SOCIETY

MNRAS **516,** 167–184 (2022) https://doi.org/10.1093/mnras/stac1339
Advance Access publication 2022 May 18

The importance of black hole repositioning for galaxy formation simulations

Yannick M. Bahé [1★], Joop Schaye [1], Matthieu Schaller [1,2], Richard G. Bower [3], Josh Borrow [3,4], Evgenii Chaikin [1], Roi Kugel,[1] Folkert Nobels [1] and Sylvia Ploeckinger[2]

[1]*Leiden Observatory, Leiden University, PO Box 9513, NL-2300 RA Leiden, the Netherlands*
[2]*Lorentz Institute for Theoretical Physics, Leiden University, PO Box 9506, NL-2300 RA Leiden, the Netherlands*
[3]*Institute for Computational Cosmology, Department of Physics, University of Durham, South Road, Durham DH1 3LE, UK*
[4]*Department of Physics, Kavli Institute for Astrophysics and Space Research, Massachusetts Institute of Technology, Cambridge, MA 02139, USA*

Accepted 2022 May 2. Received 2022 April 21; in original form 2021 September 3

ABSTRACT

Active galactic nucleus (AGN) feedback from accreting supermassive black holes (SMBHs) is an essential ingredient of galaxy formation simulations. The orbital evolution of SMBHs is affected by dynamical friction that cannot be predicted self-consistently by contemporary simulations of galaxy formation in representative volumes. Instead, such simulations typically use a simple 'repositioning' of SMBHs, but the effects of this approach on SMBH and galaxy properties have not yet been investigated systematically. Based on a suite of smoothed particle hydrodynamics simulations with the SWIFT code and a Bondi-Hoyle-Lyttleton sub-grid gas accretion model, we investigate the impact of repositioning on SMBH growth and on other baryonic components through AGN feedback. Across at least a factor ∼1000 in mass resolution, SMBH repositioning (or an equivalent approach) is a necessary prerequisite for AGN feedback; without it, black hole growth is negligible. Limiting the effective repositioning speed to $\lesssim 10\,\mathrm{km\,s^{-1}}$ delays the onset of AGN feedback and severely limits its impact on stellar mass growth in the centre of massive galaxies. Repositioning has three direct physical consequences. It promotes SMBH mergers and thus accelerates their initial growth. In addition, it raises the peak density of the ambient gas and reduces the SMBH velocity relative to it, giving a combined boost to the accretion rate that can reach many orders of magnitude. Our results suggest that a more sophisticated and/or better calibrated treatment of SMBH repositioning is a critical step towards more predictive galaxy formation simulations.

Key words: methods: numerical – galaxies: formation – galaxies: general.

1 INTRODUCTION

Energy feedback from active galactic nuclei (AGN) that are powered by supermassive black holes (SMBHs) at the centres of massive galaxies is believed to be a key driver of galaxy formation and evolution. On the observational side, evidence in support of this mechanism includes the tight relation between SMBH mass and the stellar mass or velocity dispersion of their host galaxy (e.g. Magorrian et al. 1998; McConnell & Ma 2013; Marasco et al. 2021); the presence of high-velocity gas outflows in galaxies hosting AGN (e.g. Genzel et al. 2014); and the ubiquity of low-density X-ray cavities in galaxy clusters combined with the typically low star formation rate of their central galaxies (e.g. Fabian et al. 2006; McNamara & Nulsen 2007; Hlavacek-Larrondo et al. 2012). On the theoretical side, both semi-analytic models and hydrodynamic simulations have found that the inclusion of AGN feedback is essential to reproduce observations of e.g. the stellar masses, star formation rates, and X-ray properties of massive galaxies and their host haloes (e.g. Bower et al. 2006; Booth & Schaye 2009; McCarthy et al. 2010; Crain et al. 2015; Dubois et al. 2015; Barai et al. 2018; Davé et al. 2019; Zinger et al. 2020).

In consequence, almost all contemporary simulations of massive haloes and/or large cosmological volumes contain prescriptions for the formation of, and feedback from, SMBHs (for a recent review see Vogelsberger et al. 2020). Because the characteristic sizes of SMBHs are orders of magnitude smaller than the resolution typical of current large-scale simulations such as HORIZONAGN (Dubois et al. 2014), EAGLE (Schaye et al. 2015), MAGNETICUM (Dolag et al., in preparation), ILLUSTRISTNG (Pillepich et al. 2018), or SIMBA (Davé et al. 2019), the seeding of, gas accretion on to, mergers between, and energy feedback from them must all be predicted from resolved scales by means of analytic sub-grid models. The development and improvement of these models is an active area of research (e.g. Booth & Schaye 2009; Rosas-Guevara et al. 2015; Anglés-Alcázar et al. 2017; Weinberger et al. 2017; Henden et al. 2018; Anglés-Alcázar et al. 2021; Valentini et al. 2020; Bhowmick et al. 2021), with significant differences between the effect of AGN feedback in different simulations (e.g. Davies et al. 2020; Habouzit et al. 2021; Oppenheimer et al. 2021; see also Newton & Kay 2013; Wurster & Thacker 2013 for a comparison of older models).

While this situation is broadly similar to the analogous problem of modelling feedback from star formation, there is an additional subtlety unique to AGN. Because SMBHs represent extreme local mass concentrations, any motion relative to the matter around them leads to momentum exchange via dynamical friction; this slows down

★ E-mail: bahe@strw.leidenuniv.nl

the SMBH and hence tends to make it sink towards the local potential minimum. In a collisionless background such as stars or dark matter, dynamical friction is caused by the integrated effect of gravitational two-body encounters between the SMBH and background particles, in analogy to the orbital decay of satellite subhaloes (see e.g. Taffoni et al. 2003). For SMBHs moving through a gaseous background, on the other hand, the hydrodynamic disturbance generated by their passage generates a gaseous wake, which similarly leads to a deceleration (e.g. Ostriker 1999; Beckmann, Slyz & Devriendt 2018; Morton, Khochfar & Oñorbe 2021), at least in the absence of feedback (as pointed out by e.g. Gruzinov, Levin & Matzner 2020; Toyouchi et al. 2020).

Neither of these two mechanisms emerges self-consistently from contemporary simulations, because the background cannot be sufficiently well resolved. Individual particles in such a simulation represent a large number of real stars or of any putative dark matter particles, so that the mass contrast between SMBH and background particles is artificially lowered. Together with the need to soften gravitational interactions to avoid spurious two-body relaxation, this suppresses the emergence of dynamical friction effects on SMBHs. Off-centre formation, galaxy mergers, and artificial momentum transfer from other simulated particle species would therefore lead to simulated SMBHs wandering away from the centres of galaxies to a much greater extent than observed (e.g. Reines et al. 2020; Pesce et al. 2021), or than would be expected from physical – and typically unresolved – processes such as encounters with dense molecular clouds or gravitational recoil during SMBH mergers (e.g. Campanelli et al. 2007; González et al. 2007).

For high-resolution simulations (particle masses $\lesssim 10^4\,\mathrm{M}_\odot$), several groups have recently developed models that attempt to predict and incorporate this unresolved dynamical friction component (e.g. Tremmel et al. 2015; Pfister et al. 2019; Dubois et al. 2021). These approaches differ in their implementation details as well as in which physical processes they account for. Tremmel et al. (2015), for instance, only consider gravitational dynamical friction and neglect the gas-dynamical effect, whereas Dubois et al. (2021) only account for the latter. To our knowledge, none of them (explicitly) consider the role of unresolved matter that is gravitationally bound to the SMBH, such as a nuclear star cluster or gas cloud, which enhances its effective gravitational mass (see e.g. Biernacki, Teyssier & Bleuler 2017).

In simulations of representative volumes or zoom-in simulations of galaxy clusters, however, the gap between resolved scales and those down to which dynamical friction originates from is too large and numerical convergence becomes a limiting factor (Tremmel et al. 2015). Instead, most of these simulations implicitly assume that dynamical friction is sufficiently efficient to keep SMBHs permanently near the galaxy centre; this is then enforced by periodically or continuously 'repositioning' SMBH particles towards their local potential minimum (e.g. Springel, Di Matteo & Hernquist 2005; Booth & Schaye 2009; Vogelsberger et al. 2013; Rasia et al. 2015; Schaye et al. 2015; Weinberger et al. 2017; Davé et al. 2019; Bassini et al. 2020).

Most commonly, SMBHs are repositioned to the neighbouring resolution element with the lowest gravitational potential, as done in e.g. the simulations of Springel et al. (2005), Booth & Schaye (2009), EAGLE (Schaye et al. 2015), BAHAMAS (McCarthy et al. 2017), ILLUSTRISTNG (Weinberger et al. 2017), and FABLE (Henden et al. 2018). In the latter, the SMBH velocity is additionally changed to the local mass-weighted average. In a slightly different manner, SMBHs in SIMBA (Davé et al. 2019) are repositioned to the potential minimum of their friends-of-friends (FOF) host group (provided it is not too far away), and their velocity set to the FOF centre-of-mass velocity. SMBH repositioning is also used in several higher-resolution zoom-in suites, such as APOSTLE (Sawala et al. 2016), AURIGA (Grand et al. 2017), and ARTEMIS (Font et al. 2020). Two notable exceptions using neither repositioning nor explicit forms of dynamical friction modelling for SMBHs are the HORIZONAGN (Dubois et al. 2012, 2014) and MAGNETICUM (Dolag, private communication; Steinborn et al. 2015) simulation suites. MAGNETICUM instead attempts to avoid SMBHs wandering off from the centre of their host galaxy in the first place, by seeding them at the location of the star particle with the lowest gravitational potential and avoiding strong artificial kicks during e.g. gas accretion and mergers (for details, see Hirschmann et al. 2014).

Despite its common use, the assumption of instantaneous repositioning is not justified by analytic expectations, since a typical SMBH orbit should only decay on a Gyr time-scale (Tremmel et al. 2015; Pfister et al. 2019), at least when effects other than gravitational dynamical friction from the SMBH itself are neglected. Ma et al. (2021) found that the situation is even worse for newly formed SMBH 'seeds', whose low mass should give rise to such weak dynamical friction that they are not expected to sink to the galaxy centre at all. Several recent works have highlighted the severe impacts of this overly simplistic and efficient SMBH repositioning on simulation predictions for the SMBH population themselves, such as their merger rates (e.g. Volonteri et al. 2020) or the fraction of galaxies with off-centre AGN (e.g. Bellovary et al. 2019; Boldrini, Mohayaee & Silk 2020; Bartlett et al. 2021; Bellovary et al. 2021; Ricarte et al. 2021). However, as discussed at the beginning, SMBHs are included in large-scale simulations not only – and arguably not even primarily – as objects of interest in their own right, but due to their fundamental importance for massive galaxies and their host haloes. It is conceivable that AGN feedback itself is also sensitive to the treatment of unresolved SMBH dynamics, for example due to the dependence of SMBH accretion rates on the ambient gas properties. To our knowledge, however, no detailed exploration of this dependence is reported in the literature so far, in contrast to other aspects of the SMBH model such as gas accretion (e.g. Booth & Schaye 2009; Rosas-Guevara et al. 2015; Anglés-Alcázar et al. 2017) or feedback (e.g. Sijacki et al. 2007; Crain et al. 2015; Weinberger et al. 2018; Su et al. 2021).

The objective of this paper is therefore to test the impact of a simplified SMBH dynamics modelling approach via simple repositioning on other components of the simulation. We could attempt to achieve this by comparing to a 'gold-standard' simulation with detailed, explicit modelling of dynamical friction on SMBHs. However, the required high resolution of such a run would not only make it computationally prohibitive, but also complicate comparisons to the lower-resolution simulations of interest for modelling large cosmological volumes: since galaxy formation models are typically not numerically converged (see e.g. the discussion in section 2.2 of Schaye et al. 2015), the resolution difference would inevitably introduce additional differences that are difficult to distinguish from the effect of the dynamical friction model. Instead, we will base our investigation on comparisons between simulations at fixed (intermediate and low) resolution that differ only in their modelling of SMBHs. While this approach does not permit us to identify an 'ideal' simplified way of modelling SMBH dynamics (if one even exists), it does provide a direct quantitative assessment of the difference between these prescriptions and hence the systematic uncertainty associated with their inclusion in contemporary large-scale simulations.

The remainder of this paper is structured as follows. In Section 2, we describe the simulation model and setup that we use, and then

present our comparison of different SMBH repositioning schemes in Section 3. We analyse the physical mechanisms by which repositioning affects the simulation in Section 4, before summarizing our results in Section 5. In the appendix, we present a test of artificial SMBH removal from galaxies, as well as a comparison between the SMBH model employed here and that used in the EAGLE simulations.

2 SIMULATION MODEL AND INITIAL CONDITIONS

Our simulations have been performed with SWIFT (Schaller et al. 2018), a novel *N*-body gravity and smoothed particle hydrodynamics (SPH) solver built around a fine-grained tasking framework with a hybrid parallelization approach (see Schaller et al. 2016 for a description of an earlier version).[1] The code not only achieves excellent weak and strong scaling (Borrow et al. 2018), but is also highly modular with a number of implemented gravity, hydrodynamics, and sub-grid physics schemes. Here, we use the Fast Multipole Method (Greengard & Rokhlin 1987) for gravity, fully adaptive time-steps with the Durier & Dalla Vecchia (2012) limiter, and the SPHENIX SPH scheme (Borrow et al. 2022) with the Wendland (1995) C^2 kernel and a target smoothing length of 1.2348 times the local inter-particle separation – corresponding to an average approximate neighbour number of 65 for a uniform field – as hydrodynamics solver. In the remainder of this section, we first briefly summarize our choice of sub-grid models for processes not related to SMBHs (Section 2.1), then provide a detailed description of our SMBH model (Section 2.2), and finally describe the initial conditions from which our simulations are evolved (Section 2.3).

2.1 Simulation model

Our suite of sub-grid physics models is based on those used in the OWLS (Schaye et al. 2010) and EAGLE (Schaye et al. 2015) simulations, with a number of mostly minor modifications. Apart from the SMBH model that we describe in detail below, only a succinct summary is provided here; the interested reader is referred to their detailed description and justification in Schaye et al. (2015, see also Crain et al. 2015).

Radiative cooling and photoheating are implemented on an element-by-element basis using pre-computed tables based on CLOUDY that also account for a time-dependent UV/X-ray background, inter-stellar radiation field, and self-shielding of dense gas (Ploeckinger & Schaye 2020). In contrast to the Wiersma, Schaye & Smith (2009a) tables used in EAGLE, they can model gas cooling down to a temperature of 10 K. The resolution of our simulations is, however, not sufficient to resolve the cold dense phase of the inter-stellar medium; we therefore follow Schaye & Dalla Vecchia (2008) and use an effective pressure floor (implemented as an entropy floor) with a slope of $\gamma = 4/3$ at densities $n_{\rm H} \geq 10^{-4}{\rm cm}^{-3}$, normalised[2] to $T = 8000$ K at a density $n_{\rm H} = 0.1{\rm cm}^{-3}$. Following the recent measurements by the *Planck* satellite, hydrogen reionization is assumed to occur at redshift $z = 7.5$ (Planck Collaboration VI 2020).

As in EAGLE, star formation is implemented stochastically with the Schaye & Dalla Vecchia (2008) pressure-law implementation of the Kennicutt (1998) relation between star formation rate and gas surface density. Star-forming gas particles are identified based on the properties of their sub-grid cold inter-stellar medium (ISM) phase as predicted by the Ploeckinger & Schaye (2020) cooling tables, with the sub-grid cold ISM temperature $T_{\rm sub\text{-}grid}$ taken as that corresponding to pressure and thermal equilibrium (we select the lowest one if more than one solution exists; the corresponding equilibrium density is identified as the sub-grid density). Gas particles are star forming if they are within 0.3 dex from the entropy floor and either their sub-grid temperature $T_{\rm sub\text{-}grid} < 1000$ K or their sub-grid density $n_{\rm H} > 10\,{\rm cm}^{-3}$ and simultaneously $T_{\rm sub\text{-}grid} < 10^{4.5}$ K. In practice, this selection is similar to the metallicity-dependent density threshold of Schaye (2004) that was used in EAGLE.

Energy feedback from star formation is implemented in stochastic thermal form (Dalla Vecchia & Schaye 2012), with stars of initial masses between 8 and 100 $M_\odot$ assumed to explode as core-collapse supernovae (SNe). We use the same scaling law as for EAGLE to adjust the SN energy to the birth density and metallicity of each star particle (Crain et al. 2015), but with the energy efficiency scaled between 0.5 and 5.0 (instead of 0.3–3.0) to compensate for the higher minimum SNe progenitor mass (8 instead of 6 $M_\odot$). Two further changes compared to EAGLE are that we sample the delay between star formation and feedback according to the expected life times of the SNe progenitors, and that the feedback energy is injected into the nearest gas neighbour, rather than a randomly chosen particle inside the smoothing kernel of the star particle; the latter change has a non-trivial impact as investigated in detail by Chaikin et al. (2022). We also model energy feedback from type Ia SNe and AGB stars, in addition to mass and metal injection into their surroundings based on the prescription of Wiersma et al. (2009b). Since the latter can increase the mass of individual gas particles near the centre of massive galaxies by large factors ($\gtrsim 10^3$), gas particles are split in two when their mass exceeds four times the initial baryon mass.

2.2 Modelling of supermassive black holes

Like the remainder of our sub-grid model suite, our treatment of SMBHs is based on the EAGLE model as described by Schaye et al. (2015), which is itself based on Booth & Schaye (2009) and earlier work by Springel et al. (2005). Because of the key relevance of these prescriptions to our work, and a number of changes that we have made compared to EAGLE, we now describe them in detail; they cover the seeding of SMBHs, their repositioning, mergers between them, growth by gas accretion, and the injection of feedback into their surrounding gas.

2.2.1 SMBH seeding

The initial formation of SMBH seeds is an unsolved problem and several mechanisms are considered as potentially viable (e.g. Latif & Ferrara 2016). These include remnants of Population III stars (Smith et al. 2018), direct collapse due to cooling in metal-free gas haloes (Bromm & Loeb 2003), and runaway collapse of nuclear star clusters as a consequence of gas accretion (Davies, Miller & Bellovary 2011). Common to all of them is that they cannot be modelled self-consistently at the resolution achieved by current large cosmological volumes (see Tremmel et al. 2017 for an alternative applicable to higher-resolution simulations). Since observed SMBHs clearly must have formed in some way, we therefore follow the well-established

[1] SWIFT is publicly available at http://www.swiftsim.com, including the full sub-grid physics model used here.

[2] The slope and normalization of this pressure floor are identical to those of the EAGLE Reference model, but the threshold density is lower by a factor of 10^3. This is because we no longer employ a second floor at $T = 8000$ K that was necessary in EAGLE to prevent the formation of a tenuous cold gas phase. In practice, this change has no impact on our results.

Table 1. Cosmological, resolution, and sub-grid parameters that vary between the two simulation sets used in this work. A prefix of 'c' and 'p' denotes comoving and proper lengths, respectively.

Parameter	Meaning	EAGLE-like	BAHAMAS-like
Ω_m	Matter density parameter	0.307	0.2793
Ω_Λ	Dark energy (DM) density parameter	0.693	0.7207
Ω_baryon	Baryon density parameter	0.04825	0.0463
$h \equiv H_0/(100\,\mathrm{km\,s^{-1}Mpc^{-1}})$	Reduced Hubble constant	0.6777	0.7
σ_8	RMS of the linear matter distribution on a scale $8\,h^{-1}$ cMpc	0.8288	0.821
n_s	Spectral index of primordial perturbations	0.9611	0.972
L	Box side length	25 cMpc	200 cMpc
N_initial	Initial number of DM and baryon particles (each)	376^3	360^3
m_DM	DM particle mass	$9.77 \times 10^6\,\mathrm{M}_\odot$	$5.5 \times 10^9\,\mathrm{M}_\odot$
m_baryon	Initial baryon particle mass	$1.81 \times 10^6\,\mathrm{M}_\odot$	$1.1 \times 10^9\,\mathrm{M}_\odot$
$\epsilon_\mathrm{soft,\,DM}$	Plummer-equivalent gravitational softening length (DM)	min(3.32 ckpc, 1.30 pkpc)	min(22.3 ckpc, 5.7 pkpc)
$\epsilon_\mathrm{soft,\,baryon}$	Plummer-equivalent gravitational softening length (baryons)	min(1.79 ckpc, 0.70 pkpc)	min(22.3 ckpc, 5.7 pkpc)
M_FOF	Halo mass threshold for SMBH seeding	$10^{10}\,\mathrm{M}_\odot$	$4 \times 10^{11}\,\mathrm{M}_\odot$
m_seed	SMBH seed mass	$10^4\,\mathrm{M}_\odot$	$10^5\,\mathrm{M}_\odot$
β_boost	Power-law index of the SMBH accretion boost factor	0	0.6

practice of injecting SMBH seeds by hand into sufficiently massive haloes (Springel et al. 2005).

For this purpose, we periodically run an on-the-fly FOF group finder (see Willis et al. 2020 for the implementation in SWIFT) with a linking length of 0.2 times the mean inter-particle separation, to identify haloes with a total mass above a threshold M_FOF (see Table 1). In each such halo that does not already contain at least one SMBH particle, we then convert the densest gas particle into an SMBH, which retains the mass and phase-space coordinates of its parent gas particle.

The mass of the newly formed SMBH particle is, however, not characteristic of (putative) real SMBH seeds; it is also explicitly resolution dependent and potentially already close to the $\sim 10^7\,\mathrm{M}_\odot$ scale characteristic for galaxies in which AGN feedback is important (e.g. McConnell & Ma 2013; Sahu, Graham & Davis 2019). Instead of directly associating the particle (dynamical) mass to the SMBH itself, we therefore assign a (lower) sub-grid value m_seed to the latter, which is chosen to be compatible with at least some theoretical seed formation scenarios and well below the mass scale at which AGN feedback becomes important. SMBH seeds can then be placed in appropriately low-mass haloes and grow (together with their host galaxy) until the point at which their feedback becomes important; the difference between dynamical and sub-grid mass is assumed to represent a sub-grid gas reservoir around the SMBH (see below).

The choices of the halo mass threshold for SMBH seeding M_FOF and the seed mass m_seed have a significant impact on SMBHs in low-mass galaxies (e.g. Booth & Schaye 2009), although not on the onset of rapid SMBH growth (Booth & Schaye 2009; Bower et al. 2017). We therefore calibrate these values roughly to achieve an approximately realistic SMBH mass ($\lesssim 10^5\,\mathrm{M}_\odot$) below a galaxy stellar mass of $M_\star \sim 10^{10}\,\mathrm{M}_\odot$ in our baseline model (see Table 1); the EAGLE reference model used $m_\mathrm{seed} = 1.47 \times 10^5\,\mathrm{M}_\odot$.

2.2.2 *Repositioning to account for unresolved dynamical friction*

Simulations at the resolution that we consider here can neither model dynamical friction on SMBHs self-consistently, nor can they reliably predict its effect in a sub-grid fashion (e.g. Tremmel et al. 2015). Instead, we assume that the net effect of dynamical friction is to move them towards the local potential minimum and directly impose repositioning in a simple way. First, we identify all gas and (other) SMBH particles that lie within the kernel support radius of the SMBH under consideration[3] and that are within at most three gravitational softening lengths ϵ_baryon. Out of these, we then find the particle with the lowest gravitational potential Φ_min. Our baseline model ('`Default`') is then to move the SMBH immediately to the coordinates of this particle, provided that $\Phi_\mathrm{min} < \Phi_\mathrm{SMBH}$.

This approach is similar to what was done in EAGLE and most other contemporary simulations, as discussed in the Introduction. However, there are three subtle differences of our repositioning scheme compared to EAGLE. First, the EAGLE model also allowed repositioning towards neighbouring star and dark matter particles. The reason for changing this here is purely technical; SWIFT searches for neighbours separately by type and only gas and SMBH neighbours are required for other parts of the model (see below). We have, however, performed extensive tests with a modified code version that considers all particle types for repositioning and found essentially no difference; in other words, SMBHs typically have enough nearby gas particles that these allow an efficient migration towards the potential minimum.

Secondly, in contrast to EAGLE, we apply repositioning to all SMBHs, and not only to those with a mass $m_\mathrm{BH} < 100\,m_\mathrm{gas}$. This is because even those very massive SMBHs are subject to unresolved dynamical friction, be it from additional (gas and stellar) mass bound to them, from gas-dynamical effects (Ostriker 1999), or from remaining softening of gravitational interactions with its neighbours. For the simulations presented here, this change is of little relevance: hardly any SMBHs reach such high masses.

Finally, repositioning in EAGLE – and also in many other simulations[4] such as those of Booth & Schaye (2009), BAHAMAS (McCarthy et al. 2017), and ARTEMIS (Font et al. 2020) was limited to particles moving with a speed less than $0.25\,c_\mathrm{sound}$ with respect to the SMBH,

[3]The smoothing kernel for SMBHs uses the same Wendland (1995) C^2 functional form and effective number of neighbours as for the hydrodynamics. We point out that neighbours are defined not in terms of the smoothing length h, but the radius H within which the kernel function is non-zero (see section 2.1 of Dehnen & Aly 2012). We also note that, unlike e.g. SIMBA (Davé et al. 2019), we do not impose a maximum on the SMBH smoothing length other than a technical limit of 0.5 comoving Mpc.

[4]Simulations that do *not* apply such a restriction when repositioning SMBHs include those of Springel et al. (2005, V. Springel, private communication), ILLUSTRISTNG (Weinberger et al. 2017), AURIGA (R. Grand, private communication), and SIMBA (Davé et al. 2019).

where $c_{\rm sound}$ is the sound speed of its surrounding gas (see below). This speed threshold was motivated by the desire to prevent unphysical SMBH jumps between galaxies during close flybys. We have found this worry to be largely unjustified: when such jumps occur, the fact that the velocity of the SMBH is not *directly* affected by the repositioning in our approach[5] means that it will typically move back towards its original galaxy within a few time-steps. Only for low-mass satellite galaxies is the effect more significant: their SMBHs sometimes transfer prematurely to the central galaxy during close pericentric passages. A few per cent of galaxies with $M_\star \lesssim 10^{10}\,{\rm M}_\odot$ are therefore left without an SMBH (see Appendix A). In our baseline model, we therefore allow repositioning irrespective of the velocity of the target particle. To explore the effects of this speed threshold, we also consider two variants in which repositioning is limited to particles moving at speeds less than 0.25 and $0.5\,c_{\rm sound}$ with respect to the SMBH, respectively ('`ThresholdSpeed0p25cs`' and '`ThresholdSpeed0p5cs`').

In addition to these two variants, we include models with three different repositioning approaches. The first, '`NoRepositioning`' does not apply any explicit change to SMBH positions and relies purely on the resolved dynamics of the simulation to predict their motion. This provides a comparison against which to evaluate the impact of other approaches.

Secondly, we consider an approach where the SMBH is *not immediately* moved to the position of its lowest-potential neighbour; instead, we compute the distance travelled at a putative drift speed $v_{\rm drift}$ over one time step Δt, and then move it by (at most) this distance (or less, if it is already closer to it than $v_{\rm drift}\,\Delta t$). Based on the analytic sinking time-scale of Taffoni et al. (2003), Tremmel et al. (2015), and Pfister et al. (2019), an SMBH of $m_{\rm BH} = 10^6\,{\rm M}_\odot$ in a Milky Way like galaxy has – neglecting gas-dynamical effects and additional mass bound to the SMBH – a sinking time-scale that corresponds to $v_{\rm drift} \sim 10\,{\rm km\,s^{-1}}$. Bracketing this fiducial value, we test five choices of $v_{\rm drift} = \{2, 5, 10, 50, 250\}\,{\rm km\,s^{-1}}$ and denote these models as '`DriftSpeed2kms`', '`DriftSpeed5kms`', '`DriftSpeed10kms`', '`DriftSpeed50kms`', and '`DriftSpeed250kms`', respectively.

It may be tempting to view these models as a step towards a more realistic modelling of SMBH dynamics also in relatively low resolution simulations. We emphasize, however, that this approach is none the less not particularly realistic: for example, while we impose a fixed drift speed for all SMBHs, dynamical friction should generally be stronger, and $v_{\rm drift}$ therefore higher, for more massive SMBHs and those in denser environments (the quantitative form of these dependencies is, however, less clear). Our aim here is to provide a first-order test of the sensitivity of simulation predictions to a more gradual repositioning; we therefore defer tests of more complex models to future work.

Finally, we consider a variant in which repositioning is limited to SMBHs that have not yet grown significantly, i.e. $m_{\rm BH} < 1.2\,m_{\rm seed}$ ('`SeedRepositioningOnly`'). This will allow us to differentiate between the initial repositioning of SMBH seeds from their formation site to the centre of their halo and the continuous 'pinning' of evolved SMBHs to this position.

We note that, in all simulations presented here, the potential Φ of neighbouring particles that determines where to reposition the SMBH to also includes the contribution from the SMBH itself. To our knowledge this is also the case for other simulations in which repositioning is based on the local potential minimum, but it is not actually desirable: sufficiently massive SMBHs can create a local potential minimum and therefore be prevented from repositioning towards the actual centre of their host halo. We have verified that the better approach of subtracting the contribution of the SMBH to the neighbour potential when selecting the lowest potential neighbour does not affect the results shown here. It does, however, lead to appreciably lower star formation rates of massive haloes ($M \gtrsim 10^{14}\,{\rm M}_\odot$) in low-resolution simulations, due to more efficient repositioning of their SMBH towards the halo centre – at least as long as the resolution is not so low that even the most massive black holes never grow significantly above the mass of gas particles. For new simulations, we recommend subtracting the contribution of the SMBH to the gravitational potential for the purpose of repositioning.

[5]Effectively, we have found that SMBHs come to rest in the frame of their host halo within $\lesssim$10 Myr once they have reached its potential minimum: their initial kinetic energy is rapidly lost as they attempt to climb out of the potential well, only to be continuously repositioned back to its deepest point.

2.2.3 *Mergers between SMBHs*

Through mergers, massive haloes can contain multiple SMBHs. Under favourable circumstances, two or more of these can become gravitationally bound to each other; if they can continue losing orbital energy through e.g. dynamical friction or three-body encounters with stars or gas clouds, they may eventually approach each other closely enough to emit gravitational waves and merge (e.g. Portegies Zwart & McMillan 2000; LIGO Scientific Collaboration & Virgo Collaboration 2016). The resolution of our simulations permits only a severely oversimplified modelling of this process: once a SMBH (A) comes within three baryonic softening lengths of a more massive one (B) and is also within B's kernel support radius H_B, the two are merged instantaneously if, and only if, their relative velocity Δv_{AB} is below the escape velocity from the more massive SMBH at their current distance r_{AB}: $\Delta v_{AB}^2 < 2Gm_{{\rm BH,\,B}}/r_{AB}$; i.e. if they are gravitationally bound rather than just a fly-by. Although this criterion actually better corresponds to the (slightly less restrictive) velocity threshold $\Delta v_{AB}^2 < 2G(m_{{\rm BH,\,A}} + m_{{\rm BH,\,B}})/r_{AB}$, we have verified that our results are insensitive to this difference.

This criterion is different in detail from EAGLE, where SMBH mergers required a velocity difference smaller than the circular velocity at the edge of B's smoothing kernel. Especially for SMBHs with a low ambient gas density, the kernel radius can be more than an order of magnitude larger than the gravitational softening length, so that our approach allows a larger fraction of SMBH pairs to merge (or rather, it typically allows them to merge more quickly). In a merger, we transfer the momentum, sub-grid mass, and particle mass of the lower-mass SMBH (A) to the more massive one (B), and then remove it from the simulation; this makes it straightforward to track the evolution of SMBH main progenitors back in time.

In rare situations, more than two SMBHs can be eligible to merge with each other in the same time step; there are numerous possible configurations depending on how many there are and which of them are mutually eligible to merge with each other. In such situations, each SMBH is only swallowed once, by the most massive SMBH eligible for it, and a SMBH that is due to be swallowed by one that is simultaneously swallowed itself is left intact, at least until the next time-step.

2.2.4 *Gas accretion on to SMBHs*

Apart from mergers, SMBHs grow continuously by accreting gas from their surroundings. The resolution of our simulations only

permits a crude estimate of this accretion rate $\dot{m}_{\rm BH}$ based on the spherically symmetric Bondi-Hoyle-Lyttleton model (Hoyle & Lyttleton 1939; Bondi & Hoyle 1944), limited to the Eddington (1926) rate,

$$\dot{m}_{\rm BH} = \min\left[\alpha \cdot \frac{4\pi G^2 \cdot m_{\rm BH}^2 \cdot \rho_{\rm gas}}{\left(c_{\rm sound}^2 + v_{\rm gas}^2\right)^{3/2}}, \dot{m}_{\rm Edd}\right], \quad (1)$$

where G is Newton's constant, $\rho_{\rm gas}$ and $c_{\rm sound}$ are the density and sound speed of the ambient gas, respectively, and $v_{\rm gas}$ is the bulk velocity of the gas relative to the SMBH. The latter two are computed as kernel-weighted averages over all gas neighbours while $\rho_{\rm gas}$ is computed in analogy to the density computation of gas particles by the hydrodynamics solver.[6] For gas particles within 0.3 dex of the entropy floor the temperature, and hence sound speed, is artificially raised, which could strongly suppress the estimate of $\dot{m}_{\rm BH}$; we therefore assume a sound speed corresponding to $T = 8000$ K for these particles, as appropriate for the warm volume-filling phase of the inter-stellar medium.

The limiting Eddington rate is calculated as

$$\dot{m}_{\rm Edd} = \frac{4\pi G m_{\rm p}}{\epsilon_{\rm r} c \sigma_{\rm T}} m_{\rm BH}, \quad (2)$$

with proton mass $m_{\rm p}$, radiative efficiency $\epsilon_{\rm r} = 0.1$, speed of light c, and Thomson cross-section $\sigma_{\rm T}$. Since $\dot{m}_{\rm Edd} \propto m_{\rm BH}$, Eddington-limited accretion leads to exponential SMBH growth with an e-folding time of $(\epsilon_{\rm r} c \sigma_{\rm T})/(4\pi G m_{\rm p}) = 45$ Myr (the Salpeter time).

The boost factor α in equation 1 is commonly used to compensate for the artificially low gas densities near the centre of galaxies in low-resolution simulations. Following Booth & Schaye (2009), we make α dependent on the gas density,

$$\alpha = \max\left[(n_{\rm H}/n_{\rm H}^{\star})^{\beta}, 1\right] \quad (3)$$

where $n_{\rm H}$ is the ambient number density of hydrogen atoms, $n_{\rm H}^{\star} = 0.1\,{\rm cm}^{-3}$ is a reference density above which an (unresolved) cold interstellar gas phase is expected to form (Schaye 2004), and β is a free parameter. No boost is therefore applied for SMBHs in (well-resolved) low-density environments. With $\beta = 0$, $\alpha = 1$ everywhere, i.e. the unboosted Bondi-Hoyle-Lyttleton accretion rate is used, as was the case in EAGLE (Schaye et al. 2015). We use the same setting for our intermediate-resolution simulations, but have found $\beta > 0$ necessary for low-resolution runs (see Table 1).

Different from EAGLE, our SMBH accretion model does not include a suppression factor related to the angular momentum of gas around the SMBH (Rosas-Guevara et al. 2015). There are two reasons for this change. First, it has become increasingly clear that the resolved gas kinematics around SMBHs (typically on kpc scales) are only poorly correlated with the pc scale structure of the actual accretion disc (e.g. Anglés-Alcázar et al. 2021). We therefore cannot reliably predict the angular momentum of, and hence efficiency of viscous gas transport through, the sub-grid accretion disc on which the Rosas-Guevara et al. (2015) model is based – even the Bondi radius of all but the most massive SMBHs is typically well below the resolution scale, see e.g. eq. (1) of Rosas-Guevara et al. (2015). Secondly, Bower et al. (2017, see also Dubois et al. 2015) have shown that the onset of AGN feedback, which this suppression factor was intended to regulate, is instead more fundamentally determined by the decreasing efficiency of SN feedback; whenever the latter fails to eject gas from the halo, gas densities increase and SMBHs grow rapidly, until their own feedback is able to regulate the gas content. Accordingly, we have found that calibrating the SN feedback scaling alone, in addition to the SMBH seeding parameters, provides good control of AGN feedback on intermediate mass scales. In Appendix B, we discuss the effects of this change, as well as the other main deviations in our SMBH model from EAGLE, in more detail.

Out of the total gas mass accreted over a time-step Δt, $\Delta m = \dot{m}_{\rm BH}\,\Delta t$, a fraction $\epsilon_{\rm r}$ is converted to energy (see below). The remainder, $(1-\epsilon_{\rm r})\,\Delta m$ is added to the sub-grid mass $m_{\rm BH}$ of the SMBH. If its particle mass is greater than the new $m_{\rm BH}$, the accreted mass is assumed to come from the remaining sub-grid gas reservoir when the SMBH was seeded (see above), i.e. from within the SMBH particle itself. To account for the fraction $\epsilon_{\rm r}$ of the accreted mass that is converted to energy, the dynamical SMBH mass is reduced by $\epsilon_{\rm r}\,\Delta m$ (this was not done in EAGLE).

Otherwise (i.e. if there is insufficient mass left in the sub-grid gas reservoir), the mass deficit $m_{\rm BH} + \Delta m - m_{\rm BH}^{\rm dynamical}$ (the last term denotes the dynamical mass of the SMBH) is drawn from the surrounding gas particles. In EAGLE, this was done by stochastically swallowing individual gas neighbours. This is not an ideal approach: the momentum imparted on the SMBH from the swallowed gas particle may artificially dislodge it from its position, particularly without instantaneous repositioning (as also discussed by Steinborn et al. 2015). The mass of a gas particle is also typically much greater than Δm, so that the dynamical mass of SMBH particles remains systematically above its sub-grid mass. Both issues become more severe when individual gas particles have been enriched to masses well above their initial value due to stellar outflows, which is particularly common in massive, gas-poor galaxies. Instead of swallowing entire particles, we therefore transfer a (typically very) small fraction of mass from all gas neighbours to the SMBH simultaneously, with the mass δm_i 'nibbled' from each neighbour i weighted in analogy to their contribution to the gas density at the location of the SMBH,

$$\delta m_i = (1-\epsilon_{\rm r})\Delta m \left[\frac{w_i m_i}{\sum_j (w_j m_j)}\right], \quad (4)$$

where w_i is the kernel weight of particle i, m_i its mass, and the sum is over all neighbours; as above, the factor of $(1-\epsilon_{\rm r})$ accounts for the mass converted to energy. In addition to mass, a fraction $\delta m_i/m_i$ of the momentum of neighbour i is also transferred to the SMBH. To prevent individual gas particles from becoming too light, we exclude any neighbour that would be reduced to less than half its initial mass and accept that the dynamical mass of the SMBH grows slightly less than desired in this case. In practice, we have found that this limit is never reached in the simulations presented here, because stars typically inject far more mass into gas particles than is drained by SMBHs.

2.2.5 *Thermal energy feedback from SMBHs*

To model AGN feedback, we inject energy $\Delta E = \epsilon_{\rm r}\epsilon_{\rm f}\,\Delta m\,c^2$ into the surrounding gas, where the factor $\epsilon_{\rm f}$ accounts for the (uncertain) coupling efficiency; we use $\epsilon_{\rm f} = 0.1$ throughout our simulations, but note that changes to this parameter only significantly affect the masses of SMBHs (Booth & Schaye 2009, 2010). To avoid strong numerical cooling losses (Dalla Vecchia & Schaye 2012), we follow

[6] In other words, we do not average the densities of individual neighbour particles, but estimate the gas density at the SMBH position – which is the relevant quantity in the Bondi-Hoyle-Lyttleton model – in the standard SPH way.

Booth & Schaye (2009) and heat particles by a large temperature increment $\Delta T_{\rm AGN} = 10^{8.5}$ K, which on average requires an energy $E_1 = \overline{m}_{\rm ngb}\,\Delta T_{\rm AGN} k_{\rm B}/[\mu m_{\rm p}\,(\gamma - 1)]$ per particle, where $\overline{m}_{\rm ngb}$ is the (unweighted) average mass of the gas particles within the SMBH kernel, $k_{\rm B}$ is Boltzmann's constant, $\mu = 0.59$ is the molecular mass of a fully ionized primordial gas, $m_{\rm p}$ the proton mass, and $\gamma = 5/3$ the specific heat capacity of an ideal monatomic gas. Because typically $\Delta E \ll E_1$, we store the energy in a sub-grid reservoir $E_{\rm BH}$ until $E_{\rm BH} \geq N_{\rm heat}\,E_1$. In our simulations, we exclusively use $N_{\rm heat} = 1$, but higher values have been used in previous simulations (e.g. $N_{\rm heat} = 10$ for BAHAMAS; McCarthy et al. 2017) to make the feedback more explosive. When this condition is satisfied – i.e. when there is enough energy available to heat at least $N_{\rm heat}$ average-mass neighbour particles – we heat the $N = \min(\lfloor E_{\rm BH}/E_1 \rfloor, 50, N_{\rm ngb})$ particles[7] by ΔT, where $N_{\rm ngb}$ is the total number of neighbours within the SMBH kernel, and subtract the actually used energy from $E_{\rm BH}$. To reduce the probability of having to heat more than one particle simultaneously, SMBH time-steps are limited such that the expected increase of $E_{\rm BH}$ does not exceed[8] E_1.

In the rare situation where a SMBH grows so rapidly and/or has such a long time-step that even heating $\min(N_{\rm ngb}, 50)$ average-mass neighbours would require energy $< E_{\rm BH}$, we temporarily increase $\Delta T_{\rm AGN}$ such that the entire reservoir $E_{\rm BH}$ is expected to be used up. This is different from EAGLE, where only a maximum fraction of 0.3 $N_{\rm ngb}$ was targeted for heating in any one time-step to avoid energy conservation violations in the pressure-entropy formulation of hydrodynamics used there (see appendix A1.1 of Schaye et al. 2015). The density-energy based SPHENIX hydrodynamics scheme that we use is explicitly designed and tested to not require such a limitation (Borrow et al. 2022; Borrow, Schaller & Bower 2021).

The selection of heated particles has two subtle differences compared to EAGLE. First, there is no stochasticity in how many particles we heat: as in Booth & Schaye (2009), this is directly and deterministically set by $E_{\rm BH}$ and E_1. Secondly, as for SN feedback, we heat the particle(s) closest to the SMBH rather than selecting at random within the kernel. We test the effect of the latter change in Appendix B, but refer the interested reader to Chaikin et al. (2022) for a thorough comparison between different thermal feedback injection schemes.

All simulations presented here use the same constant target heating temperature increase of $\Delta T_{\rm AGN} = 10^{8.5}$ K. For completeness, we note that our model also includes the option to use an adaptive $\Delta T_{\rm AGN}$ that scales with the SMBH mass and ambient density; this is taken as the higher of

$$\Delta T_{\rm vir} = \Delta T_{\rm ref} \left(\frac{m_{\rm BH}}{m_{\rm ref}}\right)^{2/3} \tag{5}$$

and

$$\Delta T_{\rm crit} = 10^{7.5}{\rm K} \left(\frac{n_{\rm H}}{10\,{\rm cm}^{-3}}\right)^{2/3} \left(\frac{\overline{m}_{\rm ngb}}{10^6\,{\rm M}_\odot}\right)^{1/3}, \tag{6}$$

where $\Delta T_{\rm ref}$ and $m_{\rm ref}$ are free parameters. Equation (5) is motivated by the scaling relations between SMBH and halo mass, and halo mass and virial temperature, respectively; it aims to keep $\Delta T_{\rm AGN}$ well above the halo virial temperature so that feedback-inflated bubbles can buoyantly rise from the halo centre. Equation (6) is based on Dalla Vecchia & Schaye (2012), and ensures that the feedback is not rendered numerically inefficient through immediate numerical cooling losses. Finally, $\Delta T_{\rm AGN}$ is constrained to lie in the range $[\Delta T_{\rm min}, \Delta T_{\rm max}]$. With plausible parameters $\{\Delta T_{\rm ref}, m_{\rm ref}, \Delta T_{\rm min}, \Delta T_{\rm max}\} = \{10^{8.5}\,{\rm K}, 10^8\,{\rm M}_\odot, 10^7\,{\rm K}, 10^{9.5}\,{\rm K}\}$, the simulation outcomes presented here are not noticeably different from our default choice of a constant $\Delta T_{\rm AGN} = 10^{8.5}$ K, so that we chose the latter for simplicity. It is, however, conceivable that the adaptive $\Delta T_{\rm AGN}$ prescription may be advantageous in simulations that include very massive haloes, for which high temperature increases have proven beneficial in terms of their gas content (Le Brun et al. 2014; Schaye et al. 2015; Barnes et al. 2017) and quenched galaxy fractions (Bahé et al. 2017); we will explore this in future work.

2.3 Simulation setup

With the model and its variations described above, we run two sets of periodic-volume simulations. The first uses the EAGLE L0025N0376 initial conditions as described by Schaye et al. (2015); these fill a cubic volume with a side length of 25 comoving Mpc with (initially) $N = 376^3$ gas particles of mass $m_{\rm b} = 1.81 \times 10^6\,{\rm M}_\odot$ and an equal number of DM particles with mass $m_{\rm DM} = (\Omega_m/\Omega_{\rm b} - 1)m_{\rm b} = 9.77 \times 10^6\,{\rm M}_\odot$. Motivated by Ludlow et al. (2019), who found that the use of more massive DM particles at the same softening length leads to spurious energy transfer from DM to stars, we use a (Plummer-equivalent) softening length for DM particles of 1.3 proper kpc (limited to 3.32 comoving kpc at high redshift) for DM, compared to 0.7 proper kpc (limited to 1.79 comoving kpc) for baryons. We use the same *Planck*-13 cosmology (Planck Collaboration XVI 2014) as EAGLE for these simulations; the cosmological parameters are listed in Table 1, together with the resolution characteristics and the values for those sub-grid parameters that are different between the two simulation sets.

Secondly, we run an equivalent set of simulations at the (much) lower resolution of the large-scale BAHAMAS run (McCarthy et al. 2017). These evolve a cubic volume with a side length of 200 comoving Mpc and $N = 360^3$ DM and (initial) gas particles with masses of $5.5 \times 10^9\,{\rm M}_\odot$ and $1.1 \times 10^9\,{\rm M}_\odot$, respectively. The (Plummer-equivalent) gravitational softening length is 5.7 proper kpc, limited to 22.3 comoving kpc at high redshift, for all particle species. For consistency with the initial conditions, we use the *WMAP*-9 cosmology (Hinshaw et al. 2013) here, but the small difference from the *Planck*-13 parameters is insignificant for our results. Three sub-grid parameters relating to AGN feedback have been adjusted compared to the first set to account for the lower resolution; these are listed at the bottom of Table 1.

For each set, we run 12 simulations from identical initial conditions. Ten of these correspond to the model variations listed above (`Default`, `NoRepositioning`, `ThresholdSpeed0p25cs`, `ThresholdSpeed0p5cs`, `DriftSpeed2kms`, `DriftSpeed5kms`, `DriftSpeed10kms`, `DriftSpeed50kms`, `DriftSpeed250kms`, and `SeedRepositioningOnly`). Two further variations are `NoAGN`, which is identical to `Default` except that we disable gas accretion on to, and hence feedback from, SMBHs completely; and `NoRepos_MassiveSeeds`, identical to `NoRepositioning` but with the seed mass increased by ×100. Both will be used below to interpret the results obtained from the other runs.

All simulations are evolved from initial conditions at $z = 127$ to $z = 0$, with five full snapshots stored at $z = \{2, 1, 0.5, 0.2,$

[7]The maximum value of $N = 50$ is set for technical reasons only; we have verified that it does not influence our results.

[8]There is no guarantee that $E_{\rm BH} < E_1$, because Δt is set based on the current accretion rate $\dot{m}_{\rm BH}$, while ΔE is calculated from $\dot{m}_{\rm BH}$ in the next step. To prevent extremely short time-steps for massive SMBHs accreting at a high fraction of the Eddington rate, this accretion rate dependent time step floor is not allowed to be $< 10^5$ yr.

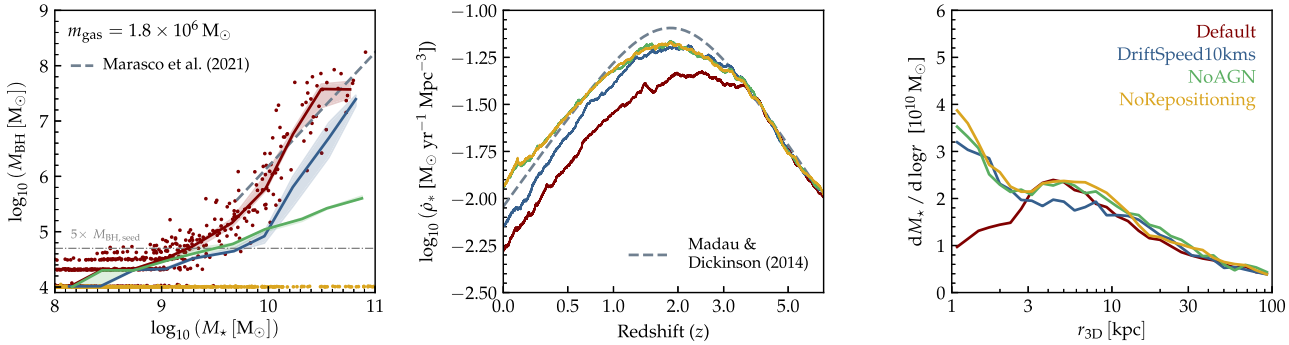

Figure 1. Comparison between different repositioning approaches for EAGLE-resolution simulations. From left to right, the three panels show the $z = 0$ stellar mass–black hole mass relation (with the horizontal grey dash–dotted line at five SMBH seed masses), the cosmic star formation rate density evolution $\dot{\rho}_\star(z)$, and the stacked $z = 0$ stellar mass profiles for haloes with $M_{\rm 200c} = [10^{12}, 10^{13}]\,{\rm M}_\odot$. Different colours represent four different models, as indicated in the top-right corner. In the left-hand and central panels, grey dashed lines denote the observational best-fitting scaling relations of Marasco et al. (2021) and Madau & Dickinson (2014), respectively; these are shown for approximate guidance only, since we have made no attempt to reproduce observational selection functions. In the left-hand panel, small circles represent individual galaxies (for clarity only shown for the `Default` and `NoRepositioning` simulations), while solid lines and shaded bands trace the running medians and their 1σ uncertainties, respectively (omitted for `NoRepositioning` to highlight the extremely small galaxy-to-galaxy scatter). Without repositioning (yellow), there is no SMBH growth or AGN feedback at all. A more gradual drifting of SMBHs towards the galaxy centre (blue) allows substantial SMBH growth, but still affects star formation far less than with instantaneous repositioning (red), especially at $z \gtrsim 1$.

0}; we use the public VELOCIRAPTOR[9] structure finder (Cañas et al. 2019; Elahi et al. 2019) to identify galaxies and haloes in each of these snapshots. A much larger number of outputs store information for only the SMBH particles, whose properties such as ambient density or accretion rate tend to fluctuate rapidly, at 5 Myr intervals.

3 THE IMPACT OF BLACK HOLE REPOSITIONING

3.1 Dependence of galaxy properties on repositioning

In Fig. 1, we compare predictions from four variants of the EAGLE-resolution simulations: `Default` (our baseline model; red), `NoRepositioning` (repositioning switched off; yellow), `DriftSpeed10kms` (instantaneous repositioning replaced by gradual drifting down the potential gradient at a fixed speed of 10 km s^{-1}; blue), and `NoAGN` (SMBH accretion, and hence also AGN feedback, switched off completely; green). From left to right, we show the relation between galaxy stellar mass $M_\star$ (the total mass of star particles bound to each galaxy within 30 proper kpc from its potential minimum) and black hole mass $M_{\rm BH}$ (defined as the sub-grid $m_{\rm BH}$ of the most massive SMBH bound to each galaxy) at $z = 0$, the redshift evolution of the cosmic star formation rate density $\dot{\rho}_\star(z)$, and the stacked $z = 0$ stellar mass profiles for the 35 haloes with mass[10] $\log_{10}(M_{\rm 200c}\,/\,{\rm M}_\odot) = [12, 13]$, i.e. towards the lower end of the range where AGN feedback is expected to have a significant impact (Bower et al. 2017; McAlpine et al. 2017).

There are several key insights from this comparison. Most significantly, *repositioning is an essential pre-requisite* for AGN feedback in our model. Without it, SMBHs experience essentially no growth at all, and both the global star formation rate history and stellar mass profiles are similar to the `NoAGN` model that explicitly disables AGN feedback. Perhaps counter-intuitively, the suppression of SMBH growth by disabling repositioning is even stronger than by switching off accretion completely (green). The reason for this is that in the latter case SMBHs can still grow by (repeated) mergers between seeds which, as a corollary, already accounts for essentially all the SMBH growth in galaxies with $M_\star \lesssim 3 \times 10^9\,{\rm M}_\odot$. The gradual repositioning model `DriftSpeed10kms` (blue), on the other hand, allows significant SMBH growth, although with a noticeable shift in the $M_{\rm BH}$–$M_\star$ relation that we explore further in Section 3.2.

In terms of the cosmic star formation rate density $\dot{\rho}_\star(z)$, our simulations show a relatively constant offset of a factor ≈3 between the `Default` and `NoRepositioning` models[11] at $z < 2$, with both runs converging at $z \gtrsim 4$ where the effect of AGN feedback is negligible. The gradual repositioning model `DriftSpeed10kms` (blue) represents a smooth transition between these two extreme cases: $\dot{\rho}_\star(z)$ closely tracks `NoAGN` until $z \approx 1.5$, and then gradually decreases more strongly, with an offset of only 0.1 dex from the instantaneous `Default` repositioning model at $z = 0$. We return to an interpretation of this feature below.

Finally, all three variations predict a similar stellar mass profile for massive $z = 0$ haloes, which are all markedly higher than in the `Default` model within the central few kpc, by a factor of 3–4. As an aside, we note that at least in terms of the stellar mass profiles, there is very little impact of AGN feedback on these galaxies beyond ≈3 kpc, comparable to their typical effective radii (e.g. Lange et al. 2015; Trujillo, Chamba & Knapen 2020).

As the careful reader may have noticed, our `Default` model predicts a cosmic star formation rate density that falls below the observed best-fitting relation of Madau & Dickinson (2014) at $z \lesssim 3$. This mismatch is not too surprising, since we have made no detailed attempt to recalibrate our sub-grid model following the updates with respect to EAGLE (Section 2); we will present such a recalibration in future work. For our purposes, the mismatch – coincidentally

[9] https://velociraptor-stf.readthedocs.io/en/latest/

[10] $M_{\rm 200c}$ is defined as the mass within the radius $r_{\rm 200c}$ inside which the mean density equals 200 times the critical density of the Universe. Note that we select haloes based on their $M_{\rm 200c}$ in a matched gravity-only simulation to ensure that we compare the exact same objects between the different models.

[11] We point out that the latter tracks the star formation rate density evolution of `NoAGN` almost perfectly, which rules out a significant impact of random run-to-run variations due to the non-deterministic nature of galaxy formation simulations at a low level (see also Genel et al. 2019; Keller et al. 2019).

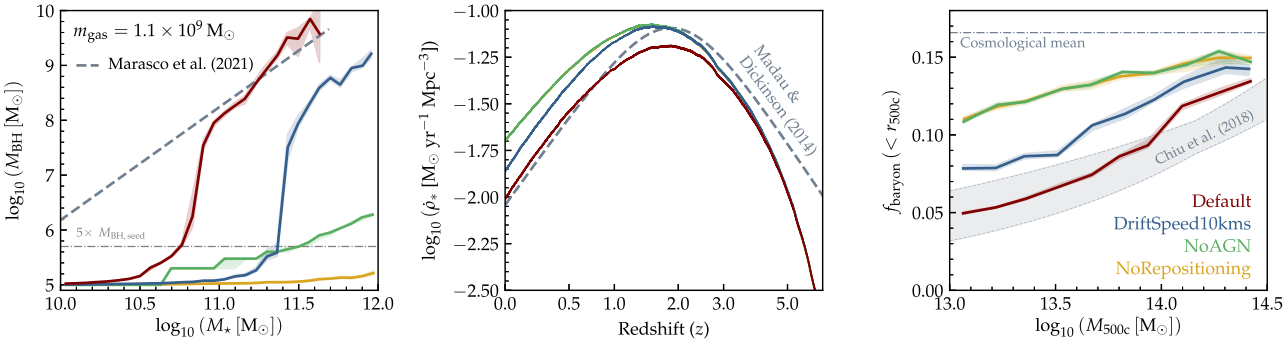

Figure 2. Comparison between different repositioning approaches for BAHAMAS-resolution simulations. The left-hand and central panels show predictions for the black hole mass–stellar mass relation and cosmic star formation rate density evolution, in analogy to Fig. 1. In the right-hand panel, the predicted baryon fractions of group/cluster haloes are plotted, with the observational relation of Chiu et al. (2018) indicated as a grey band for approximate guidance. Despite differences in detail, the conclusions are qualitatively consistent with those from our EAGLE resolution simulations: SMBH repositioning has a dramatic effect on black hole growth, star formation, and the baryon content of massive haloes.

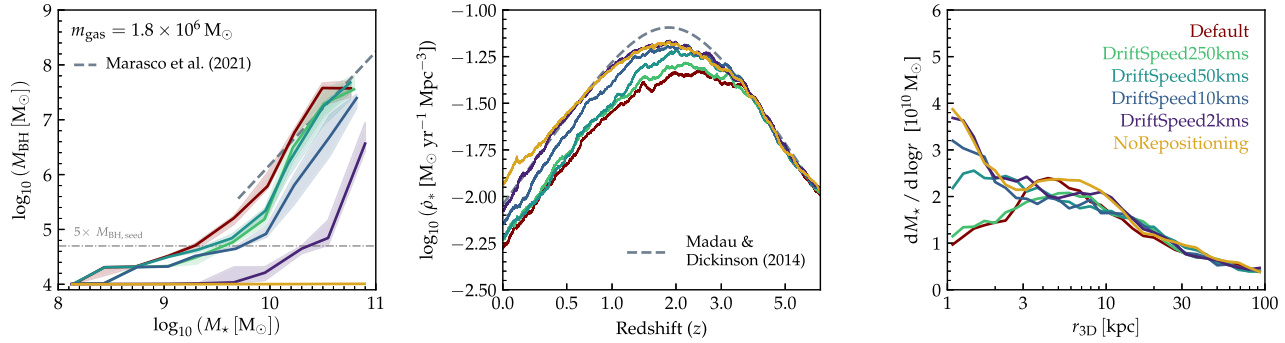

Figure 3. Similar to Fig. 1, but comparing EAGLE-resolution runs with four different drift speeds (shades of blue/green) to the `Default` (red) and `NoRepositioning` (yellow) runs. Lower SMBH drift speeds lead to systematically weaker black hole growth, later onset of AGN feedback, and higher central stellar densities in massive galaxies. Qualitatively similar trends are found in the BAHAMAS resolution simulations (not shown).

almost exactly as large as the offset between the `Default` and `NoAGN` models – is insignificant: the repositioning-related offsets are independent from it, at least to first order. To verify this explicitly, we have repeated the simulations shown in Fig. 1 with a slightly adjusted SNe feedback parametrization that results in an excellent match of $\dot\rho_\star\,(z < 2)$ to the Madau & Dickinson (2014) relation (not shown). The offsets between the four model variants agree closely with those seen from our default parametrization as used in Fig. 1 and in the rest of this paper.

To explore the sensitivity of these results to resolution and the limited volume of the EAGLE-resolution simulations, we show the analogous comparison for the BAHAMAS-resolution runs in Fig. 2; since kpc-level galaxy structures are not resolved here, we omit the stellar profiles and instead compare the baryon fractions of group/cluster-scale haloes that are missing in the small volume of the EAGLE-resolution simulations. Qualitatively, offsets between the different repositioning models are the same as for the EAGLE-resolution runs despite their three orders of magnitude difference in particle mass; the impact on the group/cluster baryon fractions mimics that on $\dot\rho_\star(z)$. In detail, the gradual drift model (`DriftSpeed10kms`, blue) deviates more strongly from the `Default` (instantaneous repositioning) approach than at EAGLE resolution, with SMBH growth strongly suppressed up to galaxy masses of $M_\star \approx 2 \times 10^{11}\,{\rm M}_\odot$; the impact on the cosmic star formation rate history is also somewhat larger (0.15 dex difference at $z = 0$). As above, `NoRepositioning` leads to negligible SMBH growth at any stellar mass and a star formation history that is nearly identical to `NoAGN`.

3.2 Gradual instead of instantaneous repositioning

Although we have argued above that a drift speed of $\sim$10 km s^{-1} is approximately consistent with typical SMBH sinking timescales under (gravitational) dynamical friction, the precise value is highly uncertain. In Fig. 3, we show the same predictions as in Fig. 1 but now comparing four (EAGLE-resolution) simulations with different drift speeds $v_{\rm drift}$ (increasing by successive factors of 5 from 2 to 250 km s^{-1}). There are clear trends with $v_{\rm drift}$ in all three panels, with `DriftSpeed2kms` closest to `NoRepositioning` and `DriftSpeed250kms` closest to `Default`. From the central panel, AGN in `DriftSpeed2kms` only affect the simulation at $z \lesssim 0.5$, whereas for `DriftSpeed250kms`, the effect on star formation is essentially the same as in the instantaneous-repositioning `Default` run at $z \lesssim 1.5$. This gradually earlier onset (and earlier full effect) of AGN feedback with higher $v_{\rm drift}$ can be understood in terms of the shorter time it takes for SMBHs to reach the galaxy centre. It corresponds to a gradually lower central stellar mass in massive haloes, while star formation beyond 3 kpc is not significantly affected. Although we only show the EAGLE-resolution simulations here, we have verified that the BAHAMAS-resolution runs show the same qualitative behaviour, consistent with our expectations from Fig. 2.

In the figures above, the $M_{\rm BH}$–$M_\star$ relation of models with gradual repositioning is systematically offset from the instantaneous-repositioning `Default` model. To understand whether this is due to an impact on the growth of stellar mass, SMBHs, or both, we plot in Fig. 4 the separate relations between both quantities and halo mass

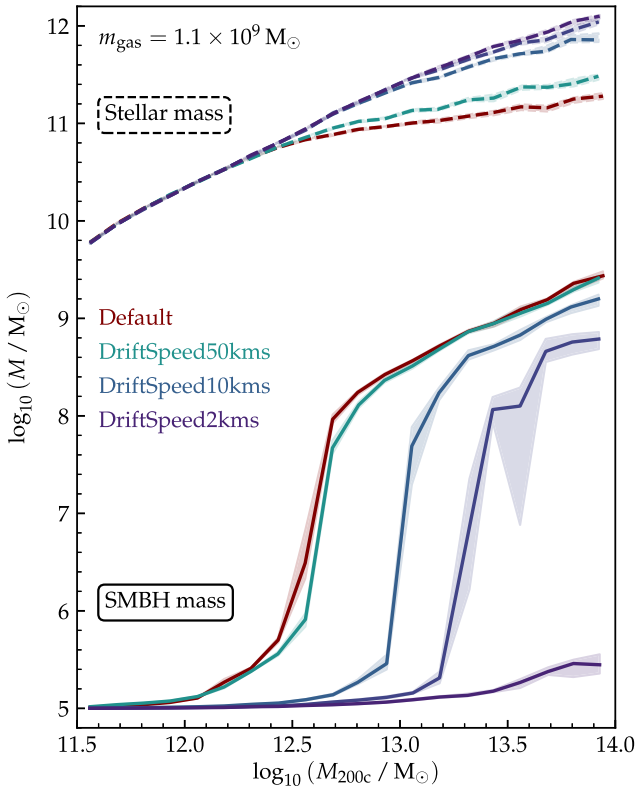

Figure 4. The effect of limiting the reposition speed on the median stellar mass (dashed lines, top) and SMBH mass (solid lines, bottom), as a function of halo mass $M_{\rm 200c}$. Lines in shades of blue and green represent four models with a fixed repositioning drift speed at BAHAMAS resolution, which are compared to the `Default` model (instantaneous repositioning, red). Shaded bands indicate 1σ bootstrapping uncertainties on the median. Reducing the repositioning speed leads to systematically higher stellar masses, shifts the rapid growth scale of SMBHs to higher halo masses, and reduces the masses of self-regulating SMBHs in massive haloes.

$M_{\rm 200c}$. We show results from the BAHAMAS-resolution simulations with the `Default` model and four variations with constant drift speed $v_{\rm drift}$ between 2 and 50 km s^{-1} (`DriftSpeed250kms` is omitted for clarity). Qualitatively consistent behaviour is seen for the equivalent EAGLE-resolution runs (not shown).

Making the SMBH repositioning non-instantaneous clearly affects both stellar and SMBH masses. Consistent with the increase in the cosmic star formation rate density seen in Fig. 3, slower repositioning (lower $v_{\rm drift}$) leads to systematically higher stellar masses. This difference increases steadily towards more massive haloes,[12] and reaches up to an order of magnitude for $M_{\rm 200c} \approx 10^{14}\,{\rm M}_\odot$. While this contributes to the offset in the $M_{\rm BH}$–$M_\star$ relation (a shift to the right for slower repositioning), there are also two clear direct effects on SMBH growth itself. First, the halo mass scale at which SMBHs experience rapid growth (Bower et al. 2017) shifts up as repositioning is slowed down, by almost a factor of 10 between $v_{\rm drift} = 50$ and 5 km s^{-1}. We defer a detailed exploration of this effect to future work, but note that one plausible mechanism is that at larger halo-centric distances (where SMBHs are typically found if repositioning is slow, see Section 4.1), gas densities are lower, so that SN feedback remains effective, and SMBH growth therefore suppressed (Bower et al. 2017) up to larger halo masses. In addition, the lower gas densities may also directly reduce SMBH growth. Alternatively, SMBHs may remain closer to the centre of more massive haloes even with slower repositioning, or differences in the build-up of haloes over cosmic time may play a role (as seen above, slower repositioning leads to a later onset of effective AGN feedback).

Secondly, the relation for massive haloes – i.e. those in which SMBHs have grown substantially, to the right of the aforementioned rapid growth point – is systematically lower for lower $v_{\rm drift}$. As discussed by Booth & Schaye (2009, see also Bower et al. 2017), SMBHs in this regime are in a state of self-regulated growth, with lower masses originating from more efficient feedback, rather than the available gas. At first, this may seem to contradict what we found above, namely that gradual drifting of SMBHs down the potential gradient (especially at low $v_{\rm drift}$) leads to a reduced impact of AGN feedback on star formation and baryon content compared to instantaneous repositioning. A plausible explanation is that smaller cooling losses in the less dense gas outside the galaxy centre (Dalla Vecchia & Schaye 2012) increase the local efficiency of AGN feedback when SMBHs are tied less strongly to the centre of their host galaxy, but that its galaxy-wide impact is diminished because the energy is injected away from the dense, star-forming core. In detail, the situation is likely even more complex, as hinted at by e.g. the qualitatively different offset between the `Default` and `DriftSpeed50kms` models for stellar and SMBH mass.

3.3 The effect of a velocity threshold for repositioning

Finally, we test the impact of limiting SMBH repositioning to slowly moving neighbour particles, as was done in some previous simulations (see above). In Fig. 5, we compare the cosmic star formation rate histories and group/cluster baryon fractions (for EAGLE and BAHAMAS resolution simulations, respectively) for the two models that include this velocity threshold, `VelocityThreshold0p25cs` and `VelocityThreshold0p5cs`.

It is evident that the velocity threshold, intended only as a guard against accidental jumps of SMBHs between galaxies, has a significant effect on the baryon distribution and star formation in the simulation. Throughout the redshift range where AGN are important ($z \lesssim 4$), the velocity threshold models predict far higher star formation rates, by more than 0.2 dex (also at the lower BAHAMAS resolution, which is not shown). The onset of AGN feedback is also delayed, to $z \approx 2$ in our simulations (the exact value is likely sensitive to other sub-grid parameters, as well as the simulation volume). At the lower resolution of BAHAMAS, the more extreme threshold ($0.25\,c_{\rm sound}$, purple) almost completely prevents AGN feedback and leads to baryon fractions close to `NoRepositioning` at $z = 0$, whereas the EAGLE resolution runs show only a very small difference between thresholds of 0.25 and 0.5 $c_{\rm sound}$. We have verified that a fixed velocity threshold of 30 km s^{-1}, independent of $c_{\rm sound}$, leads to similarly inefficient repositioning.

Like the other repositioning-related offsets, the impact of the velocity threshold may be mitigated by adjusting other sub-grid parameters. We also reiterate that there is a subtle difference between our simulations and the actual EAGLE and BAHAMAS runs in that those also allowed repositioning on to star and dark matter particles. However, it is unclear whether such parameter

[12]There is no difference in stellar mass between the different models at $\log_{10}(M_{\rm 200c}\,/\,{\rm M}_\odot) < 12.4$, even though the SMBH masses already show a clear offset at this point. This is a consequence of the low resolution of the simulations shown here: due to the large amount of energy that is required to heat even a single particle, AGN feedback can only occur once the SMBH has accreted $\sim 10^7\,{\rm M}_\odot$ of gas.

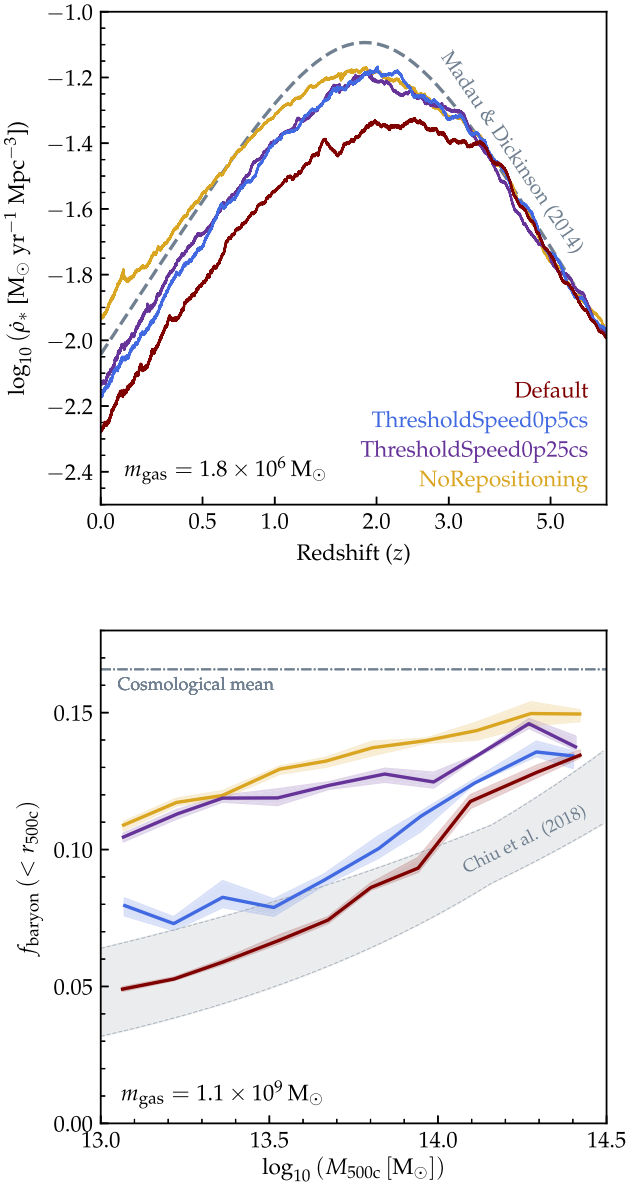

Figure 5. Star formation rate history (top panel, EAGLE resolution) and group/cluster baryon fractions (bottom panel, BAHAMAS resolution) for two simulations that limit repositioning to particles moving slowly with respect to the SMBH (blue, purple), compared to repositioning on to any particle (red) and no repositioning (yellow). The velocity threshold reduces the efficiency of AGN feedback considerably, at both resolution levels.

changes could fully compensate the velocity threshold in SMBH repositioning.

The reason for the large effect of the repositioning velocity threshold is that gas near the centre of galaxies is typically rotation-supported (at least on the scales resolved by our simulations), so that typically $v \gg c_{\rm sound}$; this is particularly true in galaxies with high central gas fractions and star formation rates. SMBHs are therefore unable to reposition until either the ambient gas temperature (and hence $c_{\rm sound}$) increases significantly – but as we have seen, AGN feedback that could cause such a temperature increase itself requires repositioning – or a temporary disruption to the velocity structure of the gas through e.g. a (galaxy) merger. Our results suggest that this (unintended) side effect of a repositioning velocity threshold should preclude its use in future simulations and warrant careful interpretation of results from simulations that did include it.

4 HOW DOES BLACK HOLE REPOSITIONING AFFECT GALAXIES?

We have shown above that SMBH repositioning (or an equivalent way of ensuring that they can sink towards the local potential minimum) is an essential prerequisite for efficient AGN feedback in intermediate- and low-resolution simulations; furthermore, repositioning is not just an 'on-off' switch as the details of its implementation matter significantly. We now investigate *why* it is so important: we first test its impact on the positions and merging of SMBHs (Section 4.1), and then on their gas accretion rates (Section 4.2).

As a preliminary step, we test *at which stage* of SMBH growth repositioning is important: to allow an initial migration to the galaxy centre after seeding, to help SMBHs acquire sufficient mass for Bondi-Hoyle-Lyttleton accretion to become efficient, or throughout their life times? For this, we compare the models `SeedRepositioningOnly`, in which SMBHs are only repositioned for a limited time after seeding (until their mass has grown by at least 20 per cent, i.e. typically until the first SMBH merger) and `NoRepos_MassiveSeeds`, in which repositioning is switched off but SMBHs are seeded at 100 × higher mass (i.e. $10^6\,{\rm M}_\odot$ and $10^7\,{\rm M}_\odot$ for the EAGLE and BAHAMAS resolution simulations, respectively), in Fig. 6.

At EAGLE resolution (top panel), neither of these two deviates significantly from `NoRepositioning`; AGN feedback remains insignificant throughout the simulation. The situation is less clear for the baryon fractions of massive haloes in the BAHAMAS resolution runs; while `NoRepos_MassiveSeeds` is still close to `NoRepositioning`, the `SeedRepositioningOnly` model predicts baryon fractions that are only $\lesssim 50$ per cent higher than in the `Default` (continuous) repositioning approach. From inspecting individual growth tracks of SMBHs in these massive haloes (not shown), we have found that they grow much of their mass (and inject the bulk of their feedback energy) within a short ($\lesssim$ 1 Gyr) period of time, starting from near seed mass. This is likely too rapid for the SMBHs to wander significantly away from the galaxy centre, even if repositioning ends as soon as this growth phase begins. The cosmic star formation rate density evolution in `SeedRepositioningOnly` at BAHAMAS resolution on the other hand, which is dominated by less massive haloes, is more strongly offset from `Default` (not shown). We therefore conclude that SMBH repositioning plays a particular role directly after seeding, but that it clearly influences black hole growth and AGN feedback also at later stages.

4.1 BH positions and mergers

The spatial distribution of SMBHs within their host halo is what is most directly affected by repositioning. On the left-hand side of Fig. 7, we show a visualization of its effect on the most massive halo in the EAGLE resolution simulations ($M_{200c} = 1.7 \times 10^{13}\,{\rm M}_\odot$ in the DM-only version); we compare this halo in the `Default` (left) and `NoRepositioning` (right) runs at $z = 0$.

A number of features in this comparison are worth pointing out. Perhaps surprisingly, the large-scale extent of the halo of SMBHs is *not* significantly different between the two models; SMBHs are found out to radii of >500 kpc in both cases. Closer to the centre, however, there is a marked difference (see the zoom-in insets): repositioning causes the difference between more than a dozen SMBHs distributed

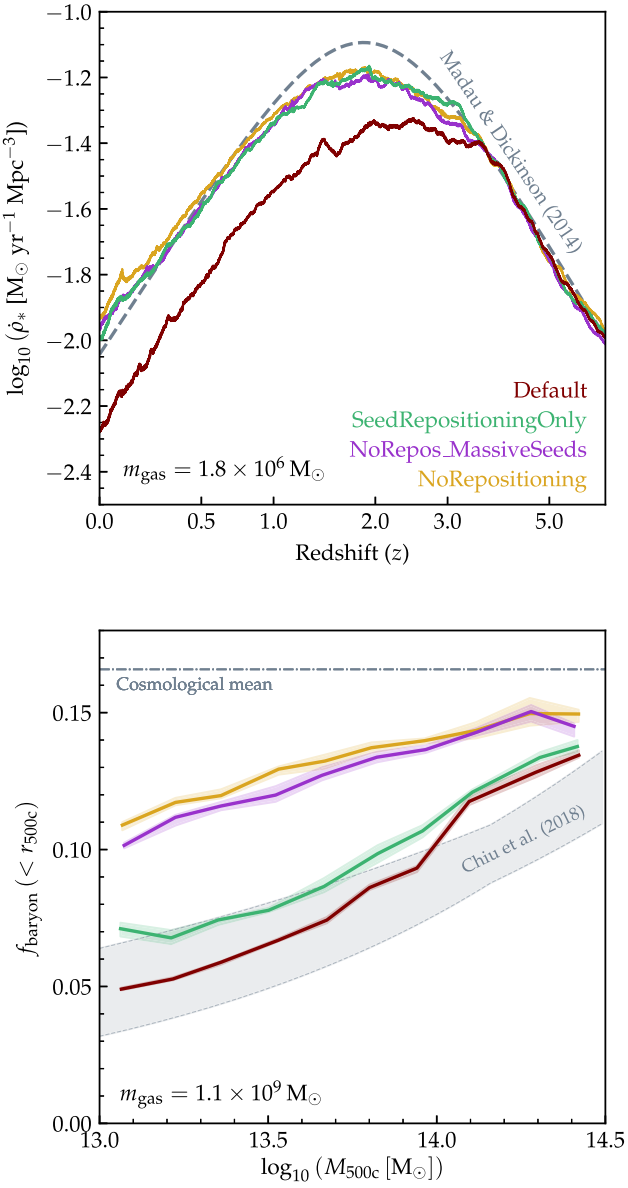

Figure 6. Star formation rate history (top panel, EAGLE resolution) and group/cluster baryon fractions (bottom panel, BAHAMAS resolution) for models `SeedRepositioningOnly` (where repositioning is only enabled while SMBHs have grown by less than 20 per cent, green) and `NoRepos_MassiveSeeds` (no repositioning but SMBHs are seeded at 100× higher mass, magenta), compared to repositioning on to any particle (red) and no repositioning (yellow). While neither of these two intermediate approaches show much of an effect in the top panel, repositioning SMBHs immediately after seeding accounts for most of its impact on the baryon content of massive haloes at BAHAMAS resolution.

throughout the central 50 kpc and a single one sitting at the very centre. Similarly, repositioning also reduces the number of SMBHs at larger radii. Consistent with Fig. 1, none of the SMBHs in the `NoRepositioning` run have grown significantly beyond the seed mass of $m_{\rm seed} = 10^4\,{\rm M}_\odot$ (dark purple colour), whereas the `Default` model has a number of SMBHs with $m_{\rm BH} \gg m_{\rm seed}$ (green/yellow points). Finally, we point out that the gas and stellar structure of the galaxy halo as shown in the background images is significantly different, as expected from our results in the previous section: without repositioning, both components show a strong central concentration, whereas the `Default` model produces a noticeably more diffuse gas halo and central group galaxy, at a level that significantly exceeds the expected variation from run-to-run stochasticity.

These differences are summarized in a more quantitative fashion by the plot on the right-hand side of Fig. 7, which shows the cumulative radial distribution function of SMBHs within all host haloes of the respective simulation at $z = 0$. In addition to the two runs depicted on the left-hand side, we also include the `DriftSpeed10kms` model here; recall that this drifts SMBHs more gradually towards the local potential minimum than the instantaneous repositioning of our `Default` model. While all three converge at the far end (with maximum SMBH distances of ≈500 kpc), weaker repositioning leads to a larger number of SMBHs at all smaller radii; in total, the `NoRepositioning` and `DriftSpeed10kms` runs contain a factor of ≈2 and ≈1.5 times more SMBHs than `Default` at $z = 0$.

The seeding of SMBHs is largely independent of repositioning, so that these differences suggest a (strong) effect on SMBH merger rates. This is not surprising, given that our SMBH merger criterion requires BHs to approach one another closely in phase-space, precisely what repositioning achieves, and also implies that simulation predictions for gravitational waves from SMBH mergers (e.g. Salcido et al. 2016) are strongly affected by repositioning. The dotted lines in the right-hand panel of Fig. 7 account for such mergers by weighting each SMBH by the number of seeds it contains, i.e. the total number of mergers that have contributed to its growth (for `NoRepositioning`, the dotted and solid blue lines lie on top of each other). As expected, these lines do all converge at small radii, confirming that the total number of SMBHs that were seeded is similar across the models. The comparison between these merger-corrected distributions then clearly reveals the expected impact of repositioning; with increasing efficiency, SMBHs are located closer to the halo centre (with the medians ranging between 10 kpc for `NoRepositioning` and 0.5 kpc for `Default`). For the halo shown on the left-hand side of Fig. 7, there are a total of 144 SMBH–SMBH mergers in the `Default` run, but not a single one in the `NoRepositioning` variant. Although only the distributions at $z = 0$ are shown for clarity, we have verified that a qualitatively consistent picture is seen at $z = 1$ and $z = 2$.

Since repositioning increases the number of SMBH mergers, a natural next question is to what extent this alone can explain the different SMBH masses and – since Bondi-Hoyle-Lyttleton accretion depends strongly on $m_{\rm BH}$ – AGN feedback efficiencies between the different models.[13] While it is evident from Fig. 1 that mergers play *some* role in the growth of SMBHs – they are the only option for SMBH growth in the `NoAGN` run – we show in Fig. 8 that they are nevertheless strongly sub-dominant to (direct) gas accretion for $m_{\rm BH} \gtrsim 10^6\,{\rm M}_\odot$; even in the `Default` model, around 95 per cent of the mass in SMBHs with $m_{\rm BH} = 10^7\,{\rm M}_\odot$ comes from gas accretion on to the main progenitor, rather than from merged SMBHs. Although less efficient repositioning (and hence fewer SMBH mergers) increases the fraction of accretion-driven growth yet further, there is therefore little room for substantial differences between the repositioning models in this respect.[14]

[13] For clarity, we emphasize that we here only refer to (sub-grid) mergers between different SMBHs. Galaxy mergers are also expected to have a significant impact on the gas-accretion driven growth of SMBHs, as discussed extensively in the literature (e.g. Hopkins et al. 2008; McAlpine et al. 2018; Lapiner, Dekel & Dubois 2021).

[14] We point out, however, that Fig. 8 only considers the total mass growth over the entire simulation; it is well conceivable that SMBH mergers play a larger

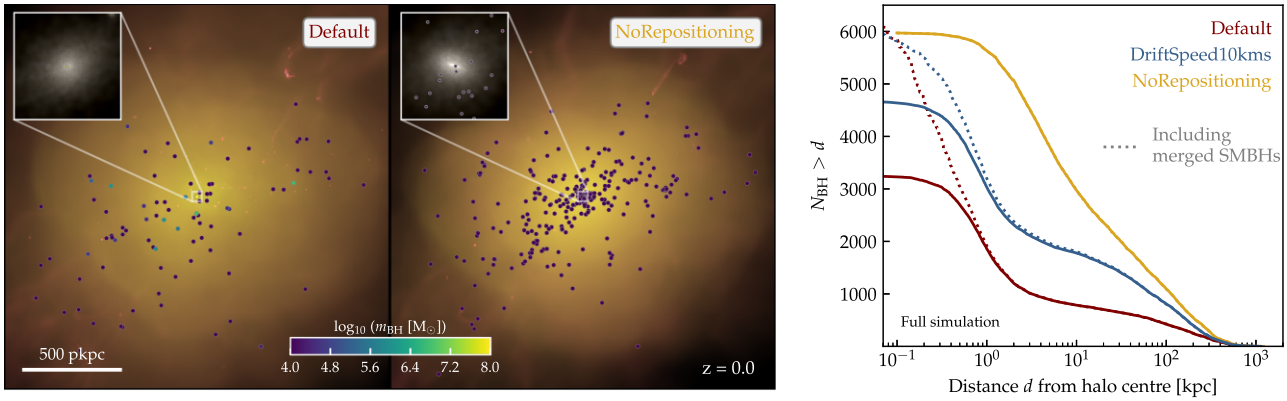

Figure 7. Projected SMBH positions (circles, colour-coded by $m_{\rm BH}$) are plotted over the corresponding gas density-temperature map (brightness representing surface density and hue temperature, increasing from pink to yellow) of the most massive $z = 0$ halo ($M_{200c} = 1.7 \times 10^{13}$ M$_\odot$) in the 25 Mpc EAGLE-resolution simulations with the `Default` (left) and `NoRepositioning` (centre) models, respectively. The insets show synthetic *gri* images of the central galaxy with a side length of 50 kpc. Right: cumulative radial distribution function of SMBHs with respect to the potential minimum of their host haloes in the full simulation volumes. SMBHs are spread throughout the halo irrespective of repositioning, but there is a far larger number of them in the `NoRepositioning` model, especially near the halo centre.

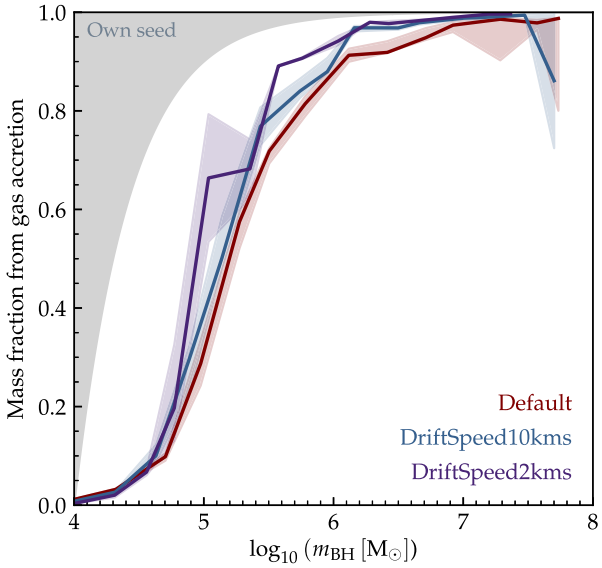

Figure 8. The fraction of SMBH mass $m_{\rm BH}$ gained through direct gas accretion, rather than from mergers with other SMBHs, for models `Default`, `DriftSpeed2kms`, and `DriftSpeed10kms`. Solid lines represent running medians, shaded bands 1σ uncertainties from bootstrap resampling. The grey area in the top-left corner indicates the region that is inaccessible due to the seed mass of the main progenitor itself. Although mergers are suppressed without efficient repositioning (Fig. 7), the effect on the growth of massive SMBHs is modest, because these gain most of their mass via gas accretion.

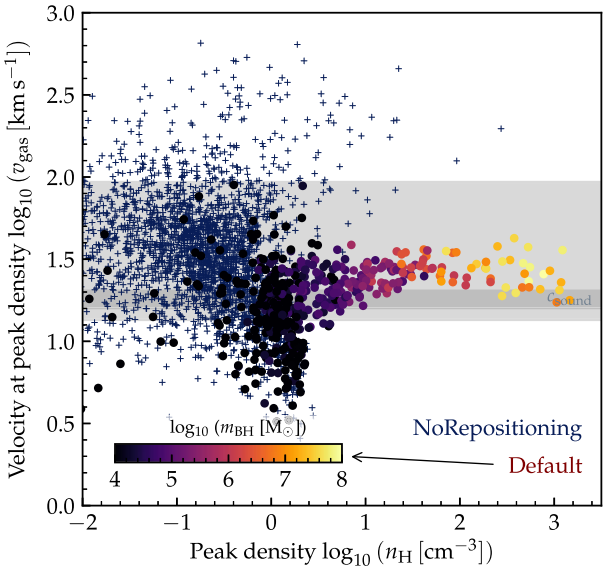

Figure 9. Peak gas density around SMBHs in haloes with $M_{200c} > 10^{11}$ M$_\odot$ at $z = 0$ (x-axis) plotted versus the ambient gas speed at this point (y-axis). Both quantities are calculated as medians over a 500 Myr interval; see text for details. The `NoRepositioning` model is shown as dark blue crosses, the `Default` model as circles whose colour indicates the final SMBH mass $m_{\rm BH}$. Dark and light grey horizontal bands cover the central 20 per cent and 68 per cent of the ambient sound speed in the latter model. Without repositioning, fewer SMBHs encounter the high densities ($n_{\rm H} \gtrsim 10\,{\rm cm}^{-3}$) required for significant growth; where they are encountered, the velocity relative to the gas is too high to permit significant accretion.

4.2 Ambient gas properties

We have seen above that weak or no repositioning leads to drastically reduced SMBH growth and AGN feedback, even when black holes are seeded at 100 times higher mass to compensate for any suppressed early growth (magenta line in Fig. 6). We have also shown that SMBH mergers contribute negligibly to the growth of those massive SMBHs that are chiefly responsible for AGN feedback. All of this suggests that gas accretion itself is strongly dependent on repositioning.

A direct comparison between accretion rates in different repositioning models is, however, non-trivial: its strong dependence on $m_{\rm BH}$ makes comparisons across SMBH masses meaningless, but as shown in Figs 1 and 2, SMBHs of the same mass live in very different large-scale environments in different models, if they exist at all. Instead, we compare in Fig. 9 the two *external* variables of the Bondi-Hoyle-Lyttleton accretion formula, i.e. ambient gas density and velocity. These could be compared at fixed redshifts across

role in the early growth of massive SMBHs. We defer a detailed investigation of this question to future work.

models, but since SMBH accretion is expected to be dominated by rapid growth phases (McAlpine et al. 2018), such a comparison would likely be dominated by 'uninteresting' SMBHs that are relatively quiescent at the time of consideration.

Instead, we make use of the high-time-resolution outputs that we store for SMBH properties (see Section 2.3) and determine for each individual SMBH the peak sustained gas density that it ever experienced. More specifically, we calculate the median density over a sliding window of 500 Myr between its seeding and $z = 0$ and record the maximum of these. This quantity is plotted on the x-axis of Fig. 9, against the median ambient gas velocity over the same time interval. For clarity, only SMBHs in haloes with $M_{200c} > 10^{11}\,\mathrm{M}_\odot$ at $z = 0$ are shown; we compare the most strongly differing models `Default` and `NoRepositioning` from the EAGLE-resolution simulations.

Two clear differences arising from SMBH repositioning are apparent. First, peak densities in the `Default` models stretch to far higher values than in `NoRepositioning`, with $n_\mathrm{H} > 1000\,\mathrm{cm}^{-3}$ in the most extreme cases. There is a clear and strong correlation between peak density and ($z = 0$) m_BH: the most massive ones are those that have experienced the highest densities. In `NoRepositioning`, on the other hand, only around a dozen SMBHs have peak densities exceeding $10\,\mathrm{cm}^{-3}$, and only two have $n_\mathrm{H} \gtrsim 100\,\mathrm{cm}^{-3}$. This is consistent with the larger halo-centric radii of SMBHs in this model (Fig. 7), since gas density decreases with radius.

Secondly, those few SMBHs that do encounter high densities without repositioning do so at much higher velocity v_peak than in the `Default` model. In the latter, v_peak is typically below 30 km s^{-1}, only marginally above the characteristic sound speed of the ambient gas. Without repositioning, on the other hand, moderately high peak densities tend to correspond to very high $v_\mathrm{peak} \gtrsim 100\,\mathrm{km\,s}^{-1}$. This is well above the sound speed and therefore controls the denominator in the expression for the Bondi-Hoyle-Lyttleton accretion rate (equation 1). Since $\dot{m}_\mathrm{BH} \propto v_\mathrm{gas}^{-3}$, this factor $\sim$10 difference in velocity corresponds to a $\sim$1000$\times$ suppression of $\dot{m}_\mathrm{BH}$, or $\sim 10^5\times$ when combined with the difference in density ($\dot{m}_\mathrm{BH} \propto n_\mathrm{H}$).

Finally, we note that both models contain a large number of SMBHs that never experience (sustained) densities above a few cm^{-3}. These also show a significant offset between the two models, with a tendency for lower peak density and higher peak velocity without repositioning. In combination, this prevents essentially any significant gas accretion without repositioning.

5 CONCLUSIONS

Large-scale cosmological hydrodynamic simulations currently require simplistic 'repositioning' prescriptions to mimic the effect of unresolved dynamical friction on supermassive black holes (SMBHs) and their AGN feedback. Unlike the prescriptions for black hole seeding, gas accretion, and AGN feedback, the effects of repositioning have not yet been investigated systematically. We have tested the impact of this repositioning on the growth of SMBHs and its associated effect on star formation and the distribution of baryons within massive haloes in a series of simulations ranging from the $\sim 10^6\,\mathrm{M}_\odot$ resolution characteristic of current galaxy formation simulations to the $\sim 10^9\,\mathrm{M}_\odot$ resolution used to model large-scale structure on cosmological scales. Gas accretion on to SMBHs is modelled with the Bondi-Hoyle-Lyttleton formula, starting from seed masses far below the SMBH mass scales of interest. Our main conclusions may be summarized as follows:

(i) Repositioning (or an equivalent explicit modelling of dynamical friction on SMBHs) is a necessary prerequisite for AGN feedback. SMBHs hardly grow in its absence, not even through mergers, with strong impacts on star formation, central stellar masses, and baryon fractions of massive haloes. Despite quantitative differences, this statement is qualitatively insensitive to resolution (Figs 1 and 2).

(ii) Replacing the instantaneous repositioning of SMBHs down the gravitational potential gradient, as is done in most contemporary simulations (e.g. EAGLE, AURIGA, BAHAMAS, ILLUSTRISTNG, FABLE, SIMBA, and ARTEMIS), with a more gradual drift of $\lesssim$10 km s^{-1} causes a significant suppression of AGN feedback. The magnitude of this suppression depends strongly on the imposed drift speed: a lower value leads to a later onset of effective AGN feedback, and hence a higher central stellar density of haloes with $M_{200c} > 10^{12}\,\mathrm{M}_\odot$, while higher values approach the outcome of instantaneous repositioning (Fig. 3).

(iii) Tying SMBHs less strongly to the centre of their host galaxies, while not disabling repositioning completely, restricts significant SMBH growth to more massive haloes. Where SMBHs can grow, they reach the state of self-regulated growth at lower masses, consistent with feedback from off-centre AGN being locally more efficient, but with a reduced impact on their host galaxy (Fig. 4).

(iv) The effect of repositioning is not limited to moving SMBHs towards the centre of their galaxy right after they are seeded, nor to allowing them to overcome slow gas accretion at low mass. Efficient AGN feedback requires repositioning of SMBHs with $m_\mathrm{BH} \gg m_\mathrm{seed}$, especially at comparatively high resolution (Fig. 6).

(v) There are three mechanisms through which repositioning affects SMBH growth, and hence AGN feedback. First, it enables SMBH mergers (Fig. 7) – which lead to higher SMBH masses and hence increase the Bondi-Hoyle-Lyttleton accretion rate – although these contribute only a minor fraction of the total mass of SMBHs with $m_\mathrm{BH} \gtrsim 10^6\,\mathrm{M}_\odot$ (Fig. 8). Secondly, it moves SMBHs to regions of higher gas density, by up to several orders of magnitude. Thirdly, it (indirectly) slows SMBHs down by an order of magnitude with respect to their ambient gas. Since the Bondi-Hoyle-Lyttleton accretion rate depends on this velocity to the third power, this suppresses gas accretion, typically by an even larger factor than due to the lower ambient gas densities (Fig. 9).

Although the impact of, and more realistic alternatives to, repositioning of SMBHs have been explored in a number of recent works based on higher-resolution simulations (e.g. Tremmel et al. 2015; Pfister et al. 2019; Ma et al. 2021), the discussion has so far focused mostly on the SMBHs themselves. In addition, all of these proposed schemes ignore the unresolved mass bound to the black hole. Our results show that this modelling detail has far wider-reaching consequences, comparable to the implementation of SMBH accretion or AGN feedback. Although it may be possible to account for the uncertainty associated with repositioning empirically through calibration of other SMBH model parameters, strong predictions for the growth of massive haloes and cosmic large-scale structure require an effort to enable the realistic modelling of SMBH dynamics across a wide range of resolutions. Alternatively, progress might be made by calibrating repositioning-related parameters (e.g. the drift speed, but also the SMBH seed mass which determines how much growth can be achieved through SMBH mergers) against observations, as is already commonly done for supernova feedback.

ACKNOWLEDGEMENTS

We thank the referee for helpful suggestions that have improved the presentation of our results, and Robert Grand, Klaus Dolag, Volker

Springel, and Rainer Weinberger for helpful clarifications about SMBH repositioning in the GADGET and AREPO simulation codes.

The authors gratefully acknowledge funding from the Netherlands Organization for Scientific Research (NWO) through Veni grant number 639.041.749, Veni grant number 639.041.751, and Vici grant number 639.043.409. This work was supported by STFC consolidated grant number ST/T000244/1. JB is supported by STFC studentship ST/R504725/1. EC is supported by the funding from the European Union's Horizon 2020 research and innovation programme under the Marie Skłodowska-Curie grant agreement no 860744. This work used the DiRAC@Durham facility managed by the Institute for Computational Cosmology on behalf of the STFC DiRAC HPC Facility (www.dirac.ac.uk). The equipment was funded by BEIS capital funding via STFC capital grants ST/K00042X/1, ST/P002293/1, ST/R002371/1, and ST/S002502/1, Durham University and STFC operations grant ST/R000832/1. DiRAC is part of the National e-Infrastructure.

The research in this paper made use of the SWIFT open-source simulation code (http://www.swiftsim.com, Schaller et al. 2018) version 0.9.0. This work made use of the PYTHON libraries NUMPY (Harris et al. 2020), MATPLOTLIB (Hunter 2007), and swiftsimio (Borrow & Borrisov 2022), and of NASA's Astrophysics Data System Bibliographic Services.

DATA AVAILABILITY

The data shown in the plots of this paper are available at https://home.strw.leidenuniv.nl/~bahe/papers.html. The SWIFT simulation code, including the full sub-grid physics model used here and the initial conditions for the EAGLE resolution simulations, is publicly available at http://www.swiftsim.com. Simulation outputs can be obtained from the corresponding author on reasonable request.

REFERENCES

Anglés-Alcázar D., Davé R., Faucher-Giguère C.-A., Özel F., Hopkins P. F., 2017, MNRAS, 464, 2840
Anglés-Alcázar D. et al., 2021, ApJ, 917, 53
Bahé Y. M. et al., 2017, MNRAS, 470, 4186
Barai P., Gallerani S., Pallottini A., Ferrara A., Marconi A., Cicone C., Maiolino R., Carniani S., 2018, MNRAS, 473, 4003
Barnes D. J. et al., 2017, MNRAS, 471, 1088
Bartlett D. J., Desmond H., Devriendt J., Ferreira P. G., Slyz A., 2021, MNRAS, 500, 4639
Bassini L. et al., 2020, A&A, 642, A37
Beckmann R. S., Slyz A., Devriendt J., 2018, MNRAS, 478, 995
Bellovary J. M., Cleary C. E., Munshi F., Tremmel M., Christensen C. R., Brooks A., Quinn T. R., 2019, MNRAS, 482, 2913
Bellovary J. M. et al., 2021, MNRAS, 505, 5129
Bhowmick A. K. et al., 2021, MNRAS, 507, 2012
Biernacki P., Teyssier R., Bleuler A., 2017, MNRAS, 469, 295
Boldrini P., Mohayaee R., Silk J., 2020, MNRAS, 495, L12
Bondi H., Hoyle F., 1944, MNRAS, 104, 273
Booth C. M., Schaye J., 2009, MNRAS, 398, 53
Booth C. M., Schaye J., 2010, MNRAS, 405, L1
Borrow J., Borrisov A., 2020, J. Open Source Softw., 5, 2430
Borrow J., Bower R. G., Draper P. W., Gonnet P., Schaller M., 2018, preprint (arXiv:1807.01341)
Borrow J., Schaller M., Bower R. G., Schaye J., 2022, MNRAS, 511, 2367
Borrow J., Schaller M., Bower R. G., 2021, MNRAS, 505, 2316
Bower R. G., Benson A. J., Malbon R., Helly J. C., Frenk C. S., Baugh C. M., Cole S., Lacey C. G., 2006, MNRAS, 370, 645
Bower R. G., Schaye J., Frenk C. S., Theuns T., Schaller M., Crain R. A., McAlpine S., 2017, MNRAS, 465, 32
Bromm V., Loeb A., 2003, ApJ, 596, 34
Cameron E., 2011, Publ. Astron. Soc. Aust., 28, 128
Campanelli M., Lousto C. O., Zlochower Y., Merritt D., 2007, Phys. Rev. Lett., 98, 231102
Cañas R., Elahi P. J., Welker C., del P Lagos C., Power C., Dubois Y., Pichon C., 2019, MNRAS, 482, 2039
Chaikin E., Schaye J., Schaller M., Bahé Y. M., Nobels F. S. J., Ploeckinger S., 2022, MNRAS, 514, 249
Chiu I. et al., 2018, MNRAS, 478, 3072
Crain R. A. et al., 2015, MNRAS, 450, 1937
Dalla Vecchia C., Schaye J., 2012, MNRAS, 426, 140
Davé R., Anglés-Alcázar D., Narayanan D., Li Q., Rafieferantsoa M. H., Appleby S., 2019, MNRAS, 486, 2827
Davies M. B., Miller M. C., Bellovary J. M., 2011, ApJ, 740, L42
Davies J. J., Crain R. A., Oppenheimer B. D., Schaye J., 2020, MNRAS, 491, 4462
Dehnen W., Aly H., 2012, MNRAS, 425, 1068
Dubois Y., Devriendt J., Slyz A., Teyssier R., 2012, MNRAS, 420, 2662
Dubois Y. et al., 2014, MNRAS, 444, 1453
Dubois Y., Volonteri M., Silk J., Devriendt J., Slyz A., Teyssier R., 2015, MNRAS, 452, 1502
Dubois Y. et al., 2021, A&A, 651, A109
Durier F., Dalla Vecchia C., 2012, MNRAS, 419, 465
Eddington A. S., 1926, The Internal Constitution of the Stars. Cambridge University Press, Cambridge, UK
Elahi P. J., Cañas R., Poulton R. J. J., Tobar R. J., Willis J. S., Lagos C. d. P., Power C., Robotham A. S. G., 2019, Publ. Astron. Soc. Aust., 36, e021
Fabian A. C., Sanders J. S., Taylor G. B., Allen S. W., Crawford C. S., Johnstone R. M., Iwasawa K., 2006, MNRAS, 366, 417
Font A. S. et al., 2020, MNRAS, 498, 1765
Genel S. et al., 2019, ApJ, 871, 21
Genzel R. et al., 2014, ApJ, 796, 7
González J. A., Hannam M., Sperhake U., Brügmann B., Husa S., 2007, Phys. Rev. Lett., 98, 231101
Grand R. J. J. et al., 2017, MNRAS, 467, 179
Greengard L., Rokhlin V., 1987, J. Comput. Phys., 73, 325
Gruzinov A., Levin Y., Matzner C. D., 2020, MNRAS, 492, 2755
Habouzit M. et al., 2021, MNRAS, 503, 1940
Harris C. R. et al., 2020, Nature, 585, 357
Henden N. A., Puchwein E., Shen S., Sijacki D., 2018, MNRAS, 479, 5385
Hinshaw G. et al., 2013, ApJS, 208, 19
Hirschmann M., Dolag K., Saro A., Bachmann L., Borgani S., Burkert A., 2014, MNRAS, 442, 2304
Hlavacek-Larrondo J., Fabian A. C., Edge A. C., Ebeling H., Sanders J. S., Hogan M. T., Taylor G. B., 2012, MNRAS, 421, 1360
Hopkins P. F., Hernquist L., Cox T. J., Kereš D., 2008, ApJS, 175, 356
Hoyle F., Lyttleton R. A., 1939, Proc. Camb. Phil. Soc., 35, 405
Hunter J. D., 2007, Comput. Sci. Eng., 9, 90
Keller B. W., Wadsley J. W., Wang L., Kruijssen J. M. D., 2019, MNRAS, 482, 2244
Kennicutt Robert C. J., 1998, ApJ, 498, 541
Lange R. et al., 2015, MNRAS, 447, 2603
Lapiner S., Dekel A., Dubois Y., 2021, MNRAS, 505, 172
Latif M. A., Ferrara A., 2016, Publ. Astron. Soc. Aust., 33, e051
Le Brun A. M. C., McCarthy I. G., Schaye J., Ponman T. J., 2014, MNRAS, 441, 1270
LIGO Scientific Collaboration, Virgo Collaboration, 2016, Phys. Rev. Lett., 116, 061102
Ludlow A. D., Schaye J., Schaller M., Richings J., 2019, MNRAS, 488, L123
Ma L., Hopkins P. F., Ma X., Anglés-Alcázar D., Faucher-Giguère C.-A., Kelley L. Z., 2021, MNRAS, 508, 1973
Madau P., Dickinson M., 2014, ARA&A, 52, 415
Magorrian J. et al., 1998, AJ, 115, 2285
Marasco A., Cresci G., Posti L., Fraternali F., Mannucci F., Marconi A., Belfiore F., Fall S. M., 2021, MNRAS, 507, 4274
McAlpine S., Bower R. G., Harrison C. M., Crain R. A., Schaller M., Schaye J., Theuns T., 2017, MNRAS, 468, 3395
McAlpine S., Bower R. G., Rosario D. J., Crain R. A., Schaye J., Theuns T., 2018, MNRAS, 481, 3118
McCarthy I. G. et al., 2010, MNRAS, 406, 822

McCarthy I. G., Schaye J., Bird S., Le Brun A. M. C., 2017, MNRAS, 465, 2936
McConnell N. J., Ma C.-P., 2013, ApJ, 764, 184
McNamara B. R., Nulsen P. E. J., 2007, ARA&A, 45, 117
Morton B., Khochfar S., Oñorbe J., 2021, preprint (arXiv:2103.15848)
Newton R. D. A., Kay S. T., 2013, MNRAS, 434, 3606
Oppenheimer B. D., Babul A., Bahé Y., Butsky I. S., McCarthy I. G., 2021, Universe, 7, 209
Ostriker E. C., 1999, ApJ, 513, 252
Pesce D. W., Seth A. C., Greene J. E., Braatz J. A., Condon J. J., Kent B. R., Krajnović D., 2021, ApJ, 909, 141
Pfister H., Volonteri M., Dubois Y., Dotti M., Colpi M., 2019, MNRAS, 486, 101
Pillepich A. et al., 2018, MNRAS, 475, 648
Planck Collaboration VI, 2020, A&A, 641, A6
Planck Collaboration XVI, 2014, A&A, 571, A16
Ploeckinger S., Schaye J., 2020, MNRAS, 497, 4857
Portegies Zwart S. F., McMillan S. L. W., 2000, ApJ, 528, L17
Rasia E. et al., 2015, ApJ, 813, L17
Reines A. E., Condon J. J., Darling J., Greene J. E., 2020, ApJ, 888, 36
Ricarte A., Tremmel M., Natarajan P., Zimmer C., Quinn T., 2021, MNRAS, 503, 6098
Rosas-Guevara Y. M. et al., 2015, MNRAS, 454, 1038
Sahu N., Graham A. W., Davis B. L., 2019, ApJ, 876, 155
Salcido J., Bower R. G., Theuns T., McAlpine S., Schaller M., Crain R. A., Schaye J., Regan J., 2016, MNRAS, 463, 870
Sawala T. et al., 2016, MNRAS, 457, 1931
Schaller M., Gonnet P., Chalk A. B. G., Draper P. W., 2016, preprint (arXiv:1606.02738)
Schaller M., Gonnet P., Draper P. W., Chalk A. B. G., Bower R. G., Willis J., Hausammann L., 2018, Astrophysics Spurce Code Library, record ascl:1805.020
Schaye J., 2004, ApJ, 609, 667
Schaye J., Dalla Vecchia C., 2008, MNRAS, 383, 1210
Schaye J. et al., 2010, MNRAS, 402, 1536
Schaye J. et al., 2015, MNRAS, 446, 521
Sijacki D., Springel V., Di Matteo T., Hernquist L., 2007, MNRAS, 380, 877
Smith B. D., Regan J. A., Downes T. P., Norman M. L., O'Shea B. W., Wise J. H., 2018, MNRAS, 480, 3762
Springel V., Di Matteo T., Hernquist L., 2005, ApJ, 620, L79
Steinborn L. K., Dolag K., Hirschmann M., Prieto M. A., Remus R.-S., 2015, MNRAS, 448, 1504
Su K.-Y. et al., 2021, MNRAS, 507, 175
Taffoni G., Mayer L., Colpi M., Governato F., 2003, MNRAS, 341, 434
Toyouchi D., Hosokawa T., Sugimura K., Kuiper R., 2020, MNRAS, 496, 1909
Tremmel M., Governato F., Volonteri M., Quinn T. R., 2015, MNRAS, 451, 1868
Tremmel M., Karcher M., Governato F., Volonteri M., Quinn T. R., Pontzen A., Anderson L., Bellovary J., 2017, MNRAS, 470, 1121
Trujillo I., Chamba N., Knapen J. H., 2020, MNRAS, 493, 87
Valentini M. et al., 2020, MNRAS, 491, 2779
Vogelsberger M., Genel S., Sijacki D., Torrey P., Springel V., Hernquist L., 2013, MNRAS, 436, 3031
Vogelsberger M., Marinacci F., Torrey P., Puchwein E., 2020, Nature Rev. Phys., 2, 42
Volonteri M. et al., 2020, MNRAS, 498, 2219
Weinberger R. et al., 2017, MNRAS, 465, 3291
Weinberger R. et al., 2018, MNRAS, 479, 4056
Wendland H., 1995, Adv. Comput. Math., 4, 389
Wiersma R. P. C., Schaye J., Smith B. D., 2009a, MNRAS, 393, 99
Wiersma R. P. C., Schaye J., Theuns T., Dalla Vecchia C., Tornatore L., 2009b, MNRAS, 399, 574
Willis J. S., Schaller M., Gonnet P., Helly J. C., 2020, preprint (arXiv:2003.11468)
Wurster J., Thacker R. J., 2013, MNRAS, 431, 2513
Zinger E. et al., 2020, MNRAS, 499, 768

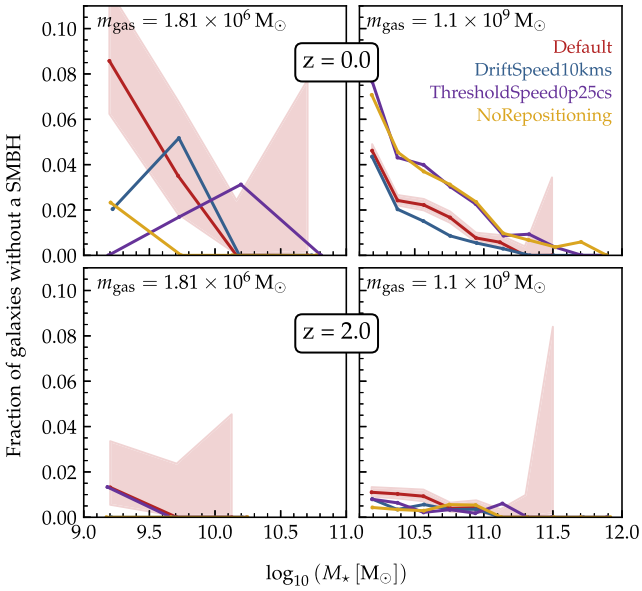

Figure A1. Fraction of galaxies that do not contain a single SMBH in four different repositioning models (different colours, see top-right panel). The top and bottom rows show results at $z = 0$ and $z = 2$, respectively, while the left and right columns are for simulations at EAGLE and BAHAMAS resolution, respectively. Shaded bands indicate binomial 1σ uncertainties following Cameron (2011); they are shown only for the `Default` model for clarity. At $z = 0$, the `Default` EAGLE resolution simulation contains a modest fraction of galaxies without SMBHs at $M_\star \lesssim 10^{10}\,{\rm M}_\odot$ due to erroneous repositioning. At higher redshift, lower resolution, or with reduced repositioning, this problem is less evident.

APPENDIX A: GALAXIES WITHOUT ANY SMBH

Although repositioning of SMBHs is intended to keep them at the centre of their host galaxy, during close encounters, it may also lead to artificial SMBH transfers to a different galaxy. We quantify the occurrence of this in Fig. A1, where we plot the fraction of galaxies that do not host a single SMBH as a function of $M_\star$, for four different repositioning models (`Default`, `DriftSpeed10kms`, `ThresholdSpeed0p25cs`, and `NoRepositioning`), two resolutions, and at two redshifts. We note first that SMBH-free galaxies occur even when repositioning is completely disabled (`NoRepositioning`, yellow), because some galaxies at the low-mass end of the ranges shown have not yet reached the required halo mass for SMBH seeding (especially in the lower-resolution simulations, where this threshold is higher).[15] However, at EAGLE resolution, SMBH-free galaxies are more common with the `Default` repositioning model at $z = 0$, at least at the low-mass end (close to 10 per cent at $M_\star \lesssim 10^{10}\,{\rm M}_\odot$). Reducing the repositioning speed (`DriftSpeed10kms`, blue) or restricting repositioning to slow-moving neighbours (`ThresholdSpeed0p25cs`, purple) generally reduces the occurrence of SMBH-free galaxies, but does not prevent them completely.

[15] We remind the reader that our SMBH seeding procedure is an extremely oversimplified model that cannot make strong predictions on the SMBH occupation fraction. While alternative prescriptions have been explored in the literature (e.g. Tremmel et al. 2017), these generally require significantly higher resolution than what is currently affordable by simulations or large representative volumes.

At $z = 2$, their occurrence is reduced to ≈1 per cent in all models, indicating that SMBH loss builds up over cosmic time. In the lower-resolution simulations, there is no clear excess of SMBH-free galaxies in the resolved mass range; in fact the `Default` model here produces fewer such cases at fixed $M_\star$. This may seem counter-intuitive at first, but can be understood in terms of the suppressed star formation efficiency such that a smaller fraction of galaxies at a given $M_\star$ fall below the SMBH seeding halo mass threshold.

We point out that the repositioning-related excess of SMBH-free galaxies is driven entirely by satellites, rather than centrals. On the one hand, this follows directly from the SMBH seeding implementation in our model: if a central somehow lost its SMBH, it would quickly be replaced by a newly seeded one. However, we have verified that none of the SMBHs that are the most massive ones in their $M_\star > 10^9\,\mathrm{M}_\odot$ galaxy were seeded after $z = 2$ in the `Default` EAGLE-resolution run, which rules out the possibility of such 'covered up' SMBH losses in centrals. Instead, we have found that SMBHs are primarily lost from satellite galaxies when they have a close pericentric passage with their central, when the SMBH is repositioned towards the central galaxy (and, typically, merged with its own SMBH), while the satellite galaxy still survives for some time.

APPENDIX B: IMPACT OF SMBH MODEL CHANGES FROM EAGLE

As discussed in Section 2, the baseline SMBH model in our simulations includes a number of updates compared to the EAGLE model described in Schaye et al. (2015). To assess the impact of these changes, we have run a number of additional simulations that revert one of these changes at a time: (i) the implementation of gas transfer from neighbouring particles (run `GasSwallowing`); (ii) calculating the sound speed for gas near the entropy floor (`RawSoundSpeed`); (iii) omitting the accretion-rate based SMBH time-step limiter (`NoBHTimeStepLimiter`); (iv) the SMBH merger criterion (`OldMergers`); (v) the choice of which neighbour particle(s) to heat in AGN feedback (`RandomAGN`); and (vi) the angular-momentum-based reduction of SMBH accretion rates (`WithAngMomLimiter`).

In Fig. B1 we compare the evolution of the cosmic star formation rate density $\dot{\rho}_\star(z)$ as predicted by these variations, for the EAGLE-resolution setup. For comparison, the `Default` and `NoAGN` models are also shown. Although there are some slight deviations between the model variations, in particular around $z = 2$, most runs track each other very closely; in other words, the changes have little impact on the global simulation outcome. The same is true for the BAHAMAS-like simulations (not shown).

The one exception is `WithAngMomLimiter` (purple), the variation that adds the angular momentum limiter term of Rosas-Guevara et al. (2015) to the Bondi-Hoyle-Lyttleton accretion formula; with it, the global star formation rate is enhanced by ≈50 per cent at $z \lesssim 2$. This is consistent with Crain et al. (2015), who showed a qualitatively similar effect in runs that varied the coupling between angular momentum and the suppression factor (their fig. 11; Valentini et al. 2020 report similar results for their independent implementation). Suitable changes to other sub-grid parameters can compensate for this difference and lead to realistic star formation histories with a standard Bondi-Hoyle-Lyttleton accretion formula.

In addition to its simpler nature, there is an empirical reason for preferring this approach to what was done in EAGLE. In Rosas-Guevara et al. (2015), the angular momentum term was found to preferentially suppress AGN feedback in low-mass galaxies when

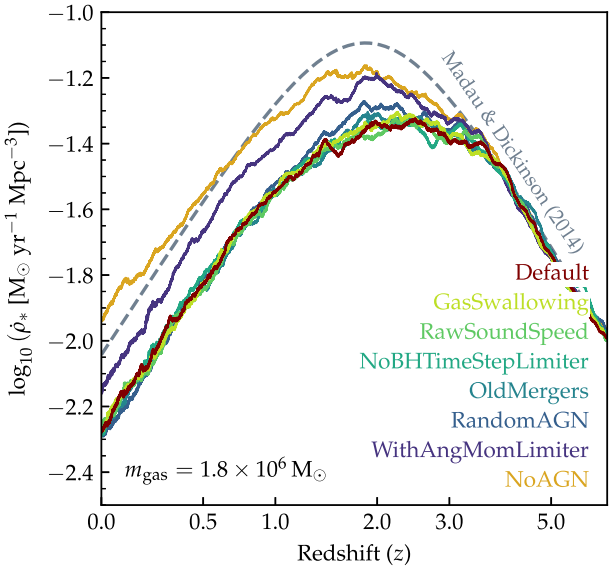

Figure B1. Global star formation rate density in EAGLE-resolution simulations that vary individual elements of our baseline SMBH model (shades of blue/green). The baseline model itself (`Default`) and the simulation with AGN feedback disabled (`NoAGN`) are shown in red and yellow, respectively. For guidance, the dashed grey line represents the observational best fit of Madau & Dickinson (2014); the simulations have not been calibrated to reproduce this. Besides `NoAGN`, the only variation that deviates significantly from the `Default` setup is `WithAngMomLimiter` (purple) that includes the angular momentum dependent SMBH accretion suppression term of Rosas-Guevara et al. (2015).

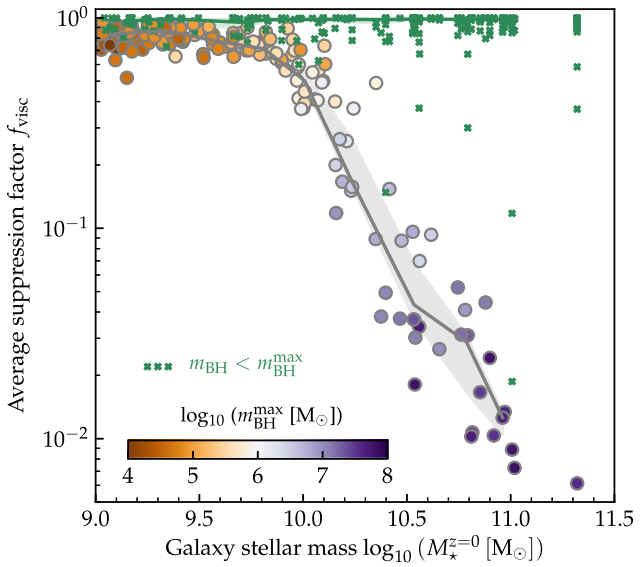

Figure B2. Dependence of the time-averaged, accretion-rate weighted SMBH accretion suppression factor f_{visc} of Rosas-Guevara et al. (2015) on galaxy stellar mass in our model, at EAGLE resolution. Large circles represent SMBHs that are the most massive ones in their halo, colour-coded according to their mass; the grey line and band traces their running median and 1σ uncertainty. Small green crosses represent other subdominant SMBHs. Contrary to expectations, f_{visc} preferentially suppresses gas accretion in the dominant SMBHs of *massive* galaxies in this simulation, by a factor of up to ∼100.

added to the sub-grid model from the OWLS project (Schaye et al. 2010). Our simulations, however, display the opposite behaviour: as shown in Fig. B2, the multiplicative factor $f_{\rm visc}$ is typically close to unity for the most massive SMBH in low-mass galaxies, but decreases systematically with stellar mass down to ≈ 0.01 at $M_\star = 10^{11}\,{\rm M}_\odot$. We speculate that this difference originates from the different stellar feedback in our simulations compared to the ones of Rosas-Guevara et al. (2015), which has a strong impact on SMBH growth (Bower et al. 2017) but also on the structure of stars and the gas that form them (Crain et al. 2015). It is conceivable that this leads to a higher degree of rotation in the central gas of massive galaxies, especially at $z \gg 0$, which is then perpetuated by the suppression of AGN feedback through the angular momentum based SMBH accretion limiter. Although only the result from the EAGLE resolution run is shown in Fig. B2, we have verified that a qualitatively similar picture emerges at BAHAMAS resolution.

This paper has been typeset from a TEX/LATEX file prepared by the author.